Quaternary Science Reviews 119 (2015) 22–34

Contents lists available at ScienceDirect

Quaternary Science Reviews

journal homepage: www.elsevier.com/locate/quascirev

The role of CO_2 decline for the onset of Northern Hemisphere glaciation

Matteo Willeit [a, *], Andrey Ganopolski [a], Reinhard Calov [a], Alexander Robinson [a, b, c], Mark Maslin [d]

[a] Potsdam Institute for Climate Impact Research, Potsdam, Germany
[b] Complutense University of Madrid, 28040 Madrid, Spain
[c] Geosciences Institute, UCM-CSIC, 28040 Madrid, Spain
[d] Department of Geography, University College London, London, UK

ARTICLE INFO

Article history:
Received 20 November 2014
Received in revised form
17 April 2015
Accepted 18 April 2015
Available online 16 May 2015

Keywords:
Paleoclimatology
Pliocene–Pleistocene transition
Northern Hemishpere glaciation
Ice sheets
Carbon dioxide
Earth system modelling

ABSTRACT

The Pliocene–Pleistocene Transition (PPT), from around 3.2 to 2.5 million years ago (Ma), represented a major shift in the climate system and was characterized by a gradual cooling trend and the appearance of large continental ice sheets over northern Eurasia and North America. Paleo evidence indicates that the PPT was accompanied and possibly caused by a decrease in atmospheric CO_2, but the temporal resolution of CO_2 reconstructions is low for this period of time and uncertainties remain large. Therefore, instead of applying existent CO_2 reconstructions we solved an 'inverse' problem by finding a schematic CO_2 concentration scenario that allows us to simulate the temporal evolution of key climate characteristics in agreement with paleoclimate records. To this end, we performed an ensemble of transient simulations with an Earth system model of intermediate complexity from which we derived a best guess transient CO_2 scenario for the interval from 3.2 to 2.4 Ma that gives the best fit between the simulated and reconstructed benthic $\delta^{18}O$ and global sea surface temperature evolution. Our data-constrained CO_2 scenarios are consistent with recent CO_2 reconstructions and suggest a gradual CO_2 decline from 375–425 to 275–300 ppm, between 3.2 and 2.4 Ma. In addition to a gradual decline, the best fit to paleoclimate data requires the existence of pronounced CO_2 variability coherent with the 41-kyr (1 kyr = 1000 years) obliquity cycle. In our simulations the long-term CO_2 decline is accompanied by a relatively abrupt intensification of Northern Hemisphere glaciation at around 2.7 Ma. This is the result of a threshold behaviour of the ice sheets response to gradual CO_2 decrease and orbital forcing. The simulated Northern Hemisphere ice sheets during the early Pleistocene glacial cycles reach a maximum volume equivalent to a sea level drop of about 40 m. Both ice volume and benthic $\delta^{18}O$ are dominated by 41-kyr cyclicity. Our simulations suggest that before 2.7 Ma Greenland was ice free during summer insolation maxima and only partly ice covered during periods of minimum summer insolation. A fully glaciated Greenland comparable to its present-day ice volume is modelled only during glacial maxima after 2.7 Ma and more continuously after 2.5 Ma.

1. Introduction

The Pliocene–Pleistocene transition (PPT) from around 3.2–3.0 to 2.5 Ma before present represented a major change in climate dynamics characterized by increased climate variability and the intensification of Northern Hemisphere glaciation (iNHG) at around 2.7 Ma (Maslin et al., 1998; Mudelsee and Raymo, 2005). Evidence for an increase in NH ice volume comes from marine sedimentary records of ice rafted debris (IRDs) (e.g. Bailey et al., 2013) and benthic $\delta^{18}O$ data (Lisiecki and Raymo, 2005).

The PPT was preceded by relatively stable and warm climatic conditions during the late-Pliocene warm period (for historical reasons still named mid-Pliocene warm period or MPWP), 3.3–3.0 Ma. It is generally believed that the late Pliocene was characterized by global temperatures 2–3 °C higher than preindustrial (Haywood and Valdes, 2004; Haywood et al., 2013). Paleoclimate data also suggest that spatial temperature contrasts where less pronounced during the Pliocene compared to the modern

* Corresponding author.
E-mail address: willeit@pik-potsdam.de (M. Willeit).

http://dx.doi.org/10.1016/j.quascirev.2015.04.015

climate. In particular, meridional sea surface temperature (SST) gradients were weaker and zonal SST gradients in the tropics almost absent (Brierley and Fedorov, 2010; Fedorov et al., 2013). Estimates of CO_2 concentrations during the late Pliocene remain very uncertain and typically range between 350 and 450 ppm (Raymo et al., 1996; Pagani et al., 2010; Seki et al., 2010). It is believed that higher CO_2 concentrations, different orography, vegetation cover and ice-sheet area contributed to the warmer Pliocene climate (Lunt et al., 2012; Willeit et al., 2013). According to various geological evidence, the peak sea level during the MPWP was 10–30 m higher than present (e.g. Miller et al., 2012), suggesting a complete absence of the Greenland and West Antarctic ice sheets and possibly some contribution from East Antarctica (Williams et al., 2010; Dolan et al., 2011; Cook et al., 2013). However, even the state of the Greenland ice sheet during the MPWP remains highly uncertain (Dolan et al., 2015).

Thereafter, paleoclimate records of SSTs distributed around the globe (Lawrence et al., 2006, 2009, 2010; Dekens et al., 2007; Medina-Elizalde et al., 2008; Etourneau et al., 2009, 2010; Brierley et al., 2009; Herbert et al., 2010; Martínez-Garcia et al., 2010; Naafs et al., 2010; Venti et al., 2013) indicate a global cooling trend, which is particularly pronounced between 3.0 and 2.5 Ma (Mudelsee and Raymo, 2005). The gradual cooling trend is also associated with an increase in the variability of benthic $\delta^{18}O$ (Lisiecki and Raymo, 2005) indicating a progressively stronger response of the climate-cryosphere system to orbital forcing. The major ice sheets over NH land seem to have appeared relatively abruptly at around 2.7 Ma as suggested by the sudden increase of IRDs at many locations in the North Atlantic, the Nordic Seas and the North Pacific around that time (Shackleton et al., 1995; Maslin et al., 1996; Jansen et al., 2000; Flesche Kleiven et al., 2002). This is possibly a result of a threshold behaviour of the ice sheets response to CO_2 and orbital forcing (Crowley and Baum, 1995; Calov and Ganopolski, 2005; Abe-Ouchi et al., 2013).

Several hypotheses for the intensification of NH glaciation have been proposed that focus on major tectonic events and their modification of both atmospheric and ocean circulation (Hay, 1992; M. Raymo, 1994; Maslin et al., 1998). These include the uplift and erosion of the Tibetan-Himalayan plateau (Ruddiman et al., 1988; Raymo, 1991; M.E. Raymo, 1994), the deepening of the Bering Straits (Einarsson et al., 1967) and/or the Greenland–Scotland ridge (Wright and Miller, 1996), the restriction of the Indonesian seaway (Cane and Molnar, 2001), and the emergence of the Panama Isthmus (Keigwin, 1978, 1982; Keller et al., 1989; Mann and Corrigan, 1990; Haug and Tiedemann, 1998).

Ruddiman et al. (1988, 1989) and Ruddiman and Kutzbach (1991) suggested that the iNHG was caused by progressive uplift of the Tibetan–Himalayan and Sierran–Coloradan regions. This may have altered the circulation of atmospheric planetary waves such that summer ablation (melting of ice accumulation) was decreased, allowing accumulation of snow and ice in the Northern Hemisphere (Boos and Kuang, 2010). However, most of the Himalayan uplift occurred much earlier between 20 Ma and 17 Ma (Copeland et al., 1987; Molnar and England, 1990) and the Tibetan Plateau reached its maximum elevation during the late Miocene (Quade et al., 1989; Harrison et al., 1992). Raymo and Ruddiman (1992), Raymo (1991, 1994) and Raymo et al. (1988) then suggested that the uplift caused increased tectonically-driven chemical weathering, which removed carbon dioxide from the atmosphere promoting global cooling.

The closure of the Panama gateway might have strengthened the Atlantic overturning circulation and warmed the North Atlantic region resulting in increased evaporation from the ocean and increased precipitation over the continents (Keigwin, 1982; Haug and Tiedemann, 1998; Bartoli et al., 2005). This creates a paradox (Berger and Wefer, 1996) as the closure of the Panama gateway would have promoted heat transfer northwards preventing or delaying glaciation of the North Hemisphere, however the increased moisture transport would have made ice sheet expansion easier. Haug and Tiedemann (1998) suggest the Panama Isthmus began to emerge at 4.6 Ma and that the gateway finally closed at 1.8 Ma. There is also evidence that the modern Atlantic–Pacific salinity contrast became fully established at 4.2 Ma, indicating a restricted surface water exchange between the two ocean basins by that time (Haug et al., 2001). There is still considerable debate on the exact timing of the Panama gateway closure (Burton et al., 1997; Frank et al., 1999; Montes et al., 2015) but it is clear that it was not the major trigger of the iNHG.

Recently, Woodard et al. (2014) suggested that the initiation of stronger heat transfer from the North Atlantic to the deep Pacific at around 2.73 Ma, possibly mediated by an increased Antarctic ice volume, could have contributed to NH glaciation by altering the interhemispheric heat and salt transport.

It was also proposed (Philander and Fedorov, 2003; Wara et al., 2005) that permanent El-Nino conditions before the iNHG could have inhibited the NH glaciation through teleconnections which caused warmer than present high latitudes. Barreiro et al. (2005) suggested that tropical Pacific temperatures associated with a permanent El-Nino state could have induced a warming and a reduction in snow cover over North America, thereby possibly preventing ice sheet growth. The switch to more sporadic El-Nino events with associated cooling would have provided conditions favourable for snow accumulation over NH land.

An increase in North Pacific stratification at around 2.7 Ma could have caused a surface ocean warming in the subarctic Pacific in autumn with consequent increased ocean evaporation and enhanced snowfall over North America in early winter (Haug et al., 2005). It also could have increased ocean carbon storage by reducing surface-to-deep exchange and therefore limiting CO_2 outgassing from the North Pacific with possible consequences on atmospheric CO_2 (Haug et al., 1999).

The most generally accepted explanation of the PPT and associated iNHG and, probably, proximal cause is the reduction of atmospheric CO_2 concentrations around this time. The changes in CO_2 through the PPT are not independent from the possible mechanisms described above, but rather could have been ultimately caused by one or more of those. Although CO_2 reconstructions for the PPT are very uncertain, there is some evidence suggesting that CO_2 decreased from the late Pliocene level of around 300–450 ppm to concentrations between 250 and 300 ppm at about 2.4 Ma (Fig. 1) and then varied somewhere between 200 and 300 ppm during the subsequent million years (Hönisch et al., 2009). Such a reduction in CO_2 would have caused a gradual global cooling resulting in increasingly favourable conditions for NH ice sheet growth. Indeed modelling experiments support the idea that a relatively modest decrease in atmospheric CO_2 could lead to the expansion of continental NH ice sheets during the PPT (Li et al., 1998; Berger et al., 1999; van de Wal et al., 2011). Lunt et al. (2008) suggest that a CO_2 decrease was also the main driver of Greenland glaciation, while other above mentioned mechanisms played only a minor role. In particular, they show that in their model an increase in snowfall alone over Greenland is not sufficient for Greenland glaciation, while the prevalence of cooler summers is a necessary condition for substantial ice sheet growth.

The time interval from 3.2 to 2.4 Ma is associated with changes in orbital forcing (Berger and Loutre, 1992), which played an important role in the iNHG (Maslin et al., 1992, 1998; Lourens and Hilgen, 1997; Haug and Tiedemann, 1998). This theory extends the ideas of Berger et al. (1993) by recognizing distinct phases during the Pleistocene and late Pliocene, characterized by the

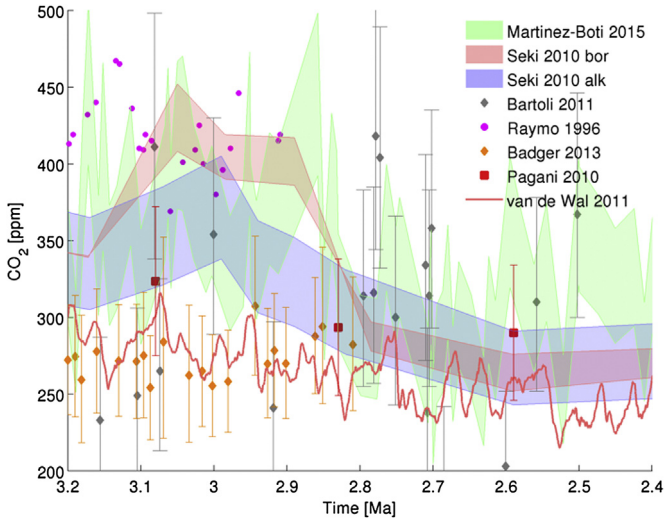

Fig. 1. CO_2 reconstructions for the PPT (Raymo et al., 1996; Pagani et al., 2010; Seki et al., 2010; Bartoli et al., 2011; Badger et al., 2013; Martínez-Botí et al., 2015). Also shown is the model-based estimate from van de Wal et al. (2011).

relative strength of the different orbital parameters during each interval. Maslin et al. (1998) and Haug and Tiedemann (1998) have suggested that the observed increase in the amplitude of orbital obliquity cycles, from 3.2 Ma onwards, may have increased seasonality of the Northern Hemisphere, thus initiating the long-term global cooling trend. The subsequent sharp rise in the amplitude of precession, and consequently, in insolation at 60°N between 2.8 Ma and 2.55 Ma may have forced the rapid glaciation of the Northern Hemisphere (Maslin et al., 1998). Though orbital forcing may have played a key role in the timing of the PPT it cannot be considered the primary cause as similar extremes occurred at 5 Ma and 7.5 Ma without large-scale glaciation of the Northern Hemisphere.

While the orbital parameters of the Earth are accurately known for the past tens of million years (Laskar et al., 2004), atmospheric CO_2 concentrations beyond the ice core age (older than 0.8 Ma) remain very uncertain (e.g. Willenbring and von Blanckenburg, 2010; Masson-Delmotte et al., 2013) and different proxies sometimes give conflicting results. This hampers testing hypotheses of the causes of the PPT and iNHG. To overcome this problem we solved an 'inverse' problem by constructing a large ensemble of schematic CO_2 pathways and then selecting scenarios that allowed us to achieve the best fit between simulated and reconstructed benthic $\delta^{18}O$ and global SST records.

2. Methods

2.1. Model

For our analysis we use the Earth system model of intermediate complexity CLIMBER-2 (Petoukhov et al., 2000; Ganopolski et al., 2001). CLIMBER-2 includes a 2.5-dimensional statistical-dynamical atmosphere model, a 3-basin zonally averaged ocean model including sea ice, the dynamic model of the terrestrial vegetation and carbon cycle VECODE (Brovkin et al., 2007, 2002, 1997) and the 3-dimensional polythermal ice sheet model SICOPOLIS (Greve, 1997) based on shallow ice approximation (Hutter, 1983; Morland, 1984). The latter is only applied for the Northern Hemisphere. The Antarctic ice sheet is prescribed according to its present day extent and elevation. The atmosphere and ice sheets are coupled bi-directionally using a physically based surface energy balance approach (Calov et al., 2005). Surface runoff and ice calving simulated by the ice sheet model are applied to the ocean as surface freshwater flux. In particular, calving is resembled as ice loss into ocean by integrating the volume per time step of all ice which is transported into the ocean by ice flux. Since the CO_2 concentration is prescribed, the marine carbon cycle model is not used in this study. Different components of the model have different spatial resolution. Atmospheric and land components have latitudinal and longitudinal resolution of 10° and approximately 51°, respectively. The ocean model has a latitudinal resolution of 2.5° and 21 vertical levels. The ice sheet model has a latitudinal resolution of 0.75°, longitudinal resolution of 1.5° and vertically 20 levels in sigma-coordinates. The CLIMBER-2 model in different configurations has been used for numerous studies of past climates: the simulation of glacial climates (Ganopolski et al., 1998; Ganopolski and Rahmstorf, 2001, 2002), hysteresis in the climate-cryosphere system (Calov and Ganopolski, 2005), the Last Glacial inception (Calov et al., 2005), glacial cycles (Ganopolski et al., 2010; Ganopolski and Calov, 2011), carbon cycle operation during the Last Glacial cycle (Brovkin et al., 2012) and the mid-Pliocene warm period (Willeit et al., 2013).

Our study includes the onset of Greenland glaciation, which occurred during the PPT. The ice sheet model used in CLIMBER-2 includes the Greenland ice sheet (GrIS), but the spatial resolution of ca 70 by 70 km is too coarse for proper simulation of the GrIS. In addition, in CLIMBER-2 the coupling between climate and ice sheet components is performed using absolute values of climate fields. These fields unavoidably contain biases and it is known that the GrIS is rather sensitive to such model biases, which is not surprising given that under preindustrial conditions the GrIS is already very close to the transition to an ice-free state (Robinson et al., 2012). To overcome this problem, we exclude Greenland from the modelling domain of the NH ice sheet model and model the GrIS evolution using the higher resolution version (20 × 20 km) of the same ice sheet model SICOPOLIS coupled to the regional climate model REMBO (Robinson et al., 2011, 2010). REMBO is a regional climate model of intermediate complexity that simulates temperature and surface mass balance of the GrIS. For the present-day lateral boundary conditions the model uses monthly ECMWF Reanalysis data (ERA-40) of 2-m temperature and relative humidity (Uppala et al., 2005), averaged over the period 1958–2001. This significantly reduces errors in simulated climate fields and mass balance over the GrIS. For climate conditions different from today, seasonal temperature anomalies from the transient simulation with CLIMBER-2 are added to the present day climatological boundary conditions. The anomalies are computed relative to a preindustrial CLIMBER-2 simulation with a prescribed ice-free Greenland and are then linearly interpolated onto the REMBO regional domain. REMBO also takes changes in orbital parameters and CO_2 concentration into account. The REMBO-SICOPOLIS model has been used for simulation of the past evolution of GrIS (Robinson et al., 2011) and its stability under global warming (Robinson et al., 2012).

The use of such a two-step approach allows us to perform much more detailed and accurate modelling of the GrIS evolution. The disadvantage of this technique is that simulated changes in the GrIS are not fed back to the global model. Climate changes outside of Greenland caused by changes of the GrIS are relatively small (e.g. Lunt et al., 2004). At the same time, simulations with ice-free Greenland show a local warming of several degrees along the Greenland boundary compared to a simulation with an ice covered Greenland (e.g. Lunt et al., 2004; Toniazzo et al., 2004). To account for the effect of changes of the GrIS spatial extent on the lateral boundary condition of REMBO, we introduced an additional temperature anomaly proportional to the simulated Greenland ice sheet area. In the standard model setup, this correction is assumed to be +2 °C for ice free Greenland and to linearly decreases to zero when the area of GrIS approaches its present-day value.

2.2. CO_2 scenarios

Based on the existing, although highly uncertain, CO_2 reconstructions for the time interval 3.2–2.4 Ma (Fig. 1), we construct generic transient CO_2 scenarios which consist of two time intervals with constant CO_2 and one interval with linearly decreasing CO_2. In addition, a component proportional to the variations of obliquity from its average value is added (Fig. 2). Mathematically the scenarios can be represented as:

$$CO_2(t) = \begin{cases} CO_2(ini) + f_{obl} \cdot \left(O(t) - \bar{O}\right), & t < t_1 \\ CO_2(ini) + (CO_2(fin) - CO_2(ini)) \dfrac{t - t_1}{t_2 - t_1} + f_{obl} \cdot \left(O(t) - \bar{O}\right), & t_1 \le t \le t_2 \\ CO_2(fin) + f_{obl} \cdot \left(O(t) - \bar{O}\right), & t > t_2 \end{cases} \quad (1)$$

where t is time, $CO_2(ini)$ and $CO_2(fin)$ are the initial and final CO_2 levels at 3.2 Ma and 2.4 Ma respectively, t_1 and t_2 delimit the time interval over which the linear CO_2 decrease applies, O is obliquity, $\bar{O}$ is the average obliquity and f_{obl} is the factor controlling the amplitude of the obliquity component of CO_2 variability. The sampled values of the five free parameters that uniquely determine the CO_2 scenarios are listed in Table 1. All possible combinations of the parameter values in Table 1 result in 540 CO_2 scenarios. Note that a scenario with constant 325 ppm CO_2 concentration is also considered for comparison, but all other scenarios imply a long term CO_2 decrease from 325–425 ppm at 3.2 Ma to 250–325 ppm at 2.4 Ma.

The obliquity component in the CO_2 scenarios is speculative because CO_2 reconstructions beyond the ice core age do not have the appropriate temporal resolution to resolve orbital-scale variability, though Ruddiman (2004, 2003) postulated that obliquity driven changes in ice volume would generate a strong positive CO_2 feedback. There are two lines of evidence in favour of the existence of a pronounced obliquity-driven component in CO_2 variability. An a priori argument is that CLIMBER-2 simulates pronounced variability in mean annual air temperature, sea ice area and deep ocean temperature at the obliquity time scale (Ganopolski and Roche, 2009) and it is known that there is a tight link between the deep ocean temperature and CO_2 concentration (Archer et al., 2004). An a posteriori argument is that without the obliquity component in CO_2, it is not possible to reach good agreement between simulated and observed time series of different climate characteristics. Note that f_{obl} does not change across the PPT which may be a conservative assumption since the observed increase in global ice volume variability with the dominant obliquity period after iNHG could also affect the CO_2 response to obliquity. However, the amplitude of obliquity variations themself increases through the PPT (Fig. 2), and consequently so does the obliquity component of the CO_2 scenarios.

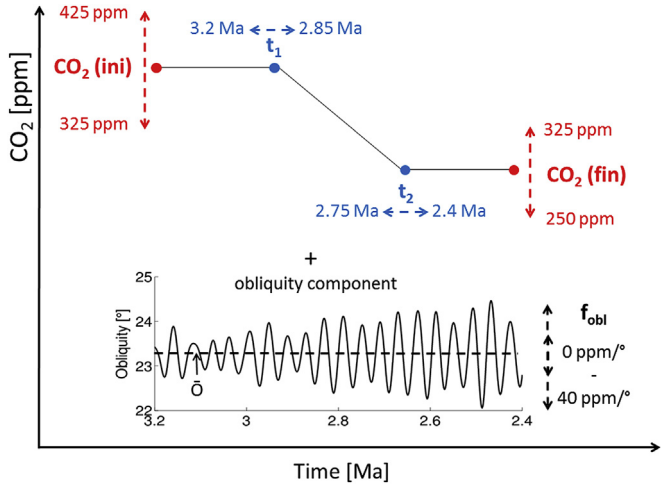

Fig. 2. Schematic illustration of the five free parameters (CO_2(ini), CO_2(fin), t_1, t_2 and f_{obl}) used to construct the CO_2 scenarios.

Note that the CLIMBER-2 radiative code treats CO_2 as the only greenhouse gas (GHG). To take into account other well-mixed GHGs, the measured CO_2 concentration is corrected by the effect of other GHGs and thus an effective CO_2 concentration has been used for the simulation of glacial cycles in Ganopolski et al. (2010) and Ganopolski and Calov (2011). Correspondingly, the CO_2 concentration derived from our modelling approach should be considered as the effective CO_2 concentration, which includes the effects of CH_4 and N_2O. It is likely however (by analogy with the last 0.8 Ma) that CO_2 dominates in our reconstructed effective CO_2 and therefore, in the following simulations, we will compare the CO_2 scenarios with available paleo CO_2 reconstructions.

2.3. Experimental setup

For each of the 540 CO_2 scenarios, we run CLIMBER-2 in transient mode from 3.22 to 2.4 Ma. The first 20,000 years are considered to be model spinup, so we only analyse results from 3.2 to 2.4 Ma. Apart from the prescribed scenarios for CO_2 concentrations, the only additional external forcing is the variation in orbital parameters. Orbital forcing is computed from the (Laskar et al., 2004) astronomical solutions (Fig. 3). All simulations are started from the climate state in equilibrium with preindustrial boundary conditions. The initial condition for the ice sheet model is an ice-free NH with a relaxed lithosphere.

The modelling procedure is structured in 4 steps:

1) First, CLIMBER-2 with prescribed ice-free Greenland is used to derive the best CO_2 scenarios, assuming that the potential Greenland contribution to the global signal recorded in the LR04 stack is small and that global SSTs are only marginally affected by the Greenland ice cover.
2) The Greenland ice sheet is then simulated separately in a second step with the regional REMBO-SICOPOLIS model driven by simulated CLIMBER-2 Greenland temperature anomalies from step 1. The Greenland simulations are performed only for the best ten CO_2 scenarios previously derived with CLIMBER-2 in step 1. We also created a 20 member REMBO-SICOPOLIS ensemble to account for model and boundary conditions uncertainties. We perturbed an ice discharge and a surface melt parameter in the range constrained by paleodata (Calov et al.,

Table 1
Sampled values for the five free parameters used to construct the CO_2 scenarios illustrated in Fig. 2.

CO_2(ini) [ppm]	CO_2(fin) [ppm]	t_1 [Ma]	t_2 [Ma]	f_{obl} [ppm/deg]
325, 350, 375, 400, 425	250, 275, 300, 325	3.2, 3.025, 2.85	2.75, 2.575, 2.4	0, 20, 40

2015) and varied the temperature anomaly introduced to account for changes in the simulated Greenland ice sheet area as described in Section 2.1 in the range 1–3 °C.

3) In a third step we explore the effect of the transient Greenland glaciations on climate and the rest of the NH ice sheets by prescribing the ice fractions of the GrIS modelled in step 2 in transient CLIMBER-2 experiments. This iteration is again performed only for the ten best CO_2 scenarios and for each member of the REMBO-SICOPOLIS model ensemble.
4) In the final step, CLIMBER-2 Greenland temperatures from step 3 are again used to force REMBO-SICOPOLIS to get the final Greenland ice sheet evolution during the PPT.

Except for the derivation of the best CO_2 scenarios, all other analyses are performed using the output of the experiments from step 3 for climate and continental ice sheets (ENS_CLIM) and from step 4 for the Greenland ice sheet (ENS_GRL).

2.4. Empirical constraints and selection of the best CO_2 scenarios

To select the best fit CO_2 scenario for the PPT we use agreement with the benthic LR04 $\delta^{18}O$ stack (Lisiecki and Raymo, 2005) and the global SST stack (Martínez-Botí et al., 2015) as criteria of realism of simulations driven by the different CO_2 scenarios. The geographic location of the marine cores which are used to derive the $\delta^{18}O$ stack for the time period 3.2–2.4 Ma and the sites of the cores where SST has been reconstructed are shown in Fig. 4.

Since CLIMBER-2 does not incorporate a comprehensive $\delta^{18}O$ model, benthic $\delta^{18}O$ is computed from the deep ocean temperature T_d and the NH ice volume expressed in terms of sea level equivalent V_{seq} using the linearized version of temperature-$\delta^{18}O$ relationship (Shackleton, 1974) and assuming a linear relation between $\delta^{18}O$ and ice volume:

$$\delta^{18}O = 4.2 - 0.25T_d - 0.011V_{seq}. \quad (2)$$

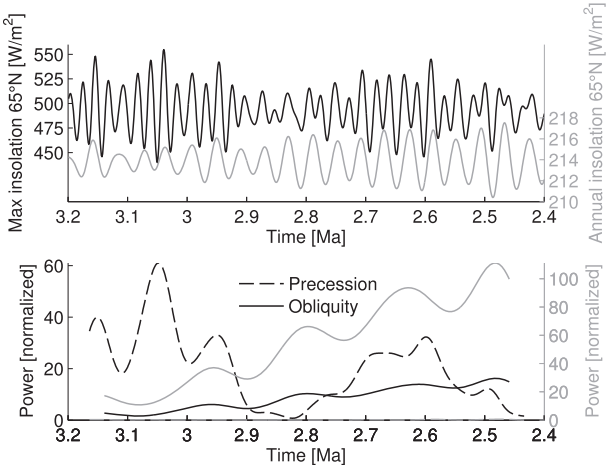

Fig. 3. Top: Maximum summer insolation at 65°N (black) and mean annual insolation at 65°N (grey) from 3.2 to 2.4 Ma. Bottom: power of the maximum summer and mean annual insolation in the frequency bands corresponding to precession (18–25 kyr), and obliquity (37–44 kyr) variations. Power is computed from a time-frequency wavelet spectrum and is normalized by the variance of the time series.

This relationship has been already used in Ganopolski and Calov (2011). Compared to comprehensive modelling of global $\delta^{18}O$, this approach is based on a number of rather strong assumptions. Firstly, the relationship between $\delta^{18}O$ in sea water may deviate from linear because average $\delta^{18}O$ composition of the ice sheets does not remain constant during glacial cycles (de Boer et al., 2012). In addition, local benthic $\delta^{18}O$ in calcites is controlled not only by global ice volume and local temperature but also by other factors, such as change in deep water formation areas and, as shown in Ganopolski and Roche (2009), local benthic $\delta^{18}O$ can lead or lag global ice volume by several thousand years. However, since we compare our modelled $\delta^{18}O$ with the global stack, the influence of these problems is less significant than for individual $\delta^{18}O$ records. There is also some uncertainty in the choice of the parameters in eq. (2). Recently Marchitto et al. (2014) suggested a slightly lower value of 0.22‰/°C for the temperature-$\delta^{18}O$ slope while values for the sea level-$\delta^{18}O$ slope commonly used are in the range 0.09–0.011 ‰/msl (de Boer et al., 2012).

A more serious problem may be represented by the fact that the Antarctic ice sheet is not included in our modelling setup and changes in Antarctic ice volume are not taken into account. Antarctic contribution to the late Pliocene sea level highstands is not accurately known, but the upper estimate of 20 m above present day sea level given in Masson-Delmotte et al. (2013) would imply Antarctic contribution of about 10 m in sea level equivalent or 0.1‰ of $\delta^{18}O$. Contribution of Antarctic ice sheet to the magnitude of global ice volume variations on the orbital periods is also not known. During recent (and the strongest) glacial cycles, Antarctic

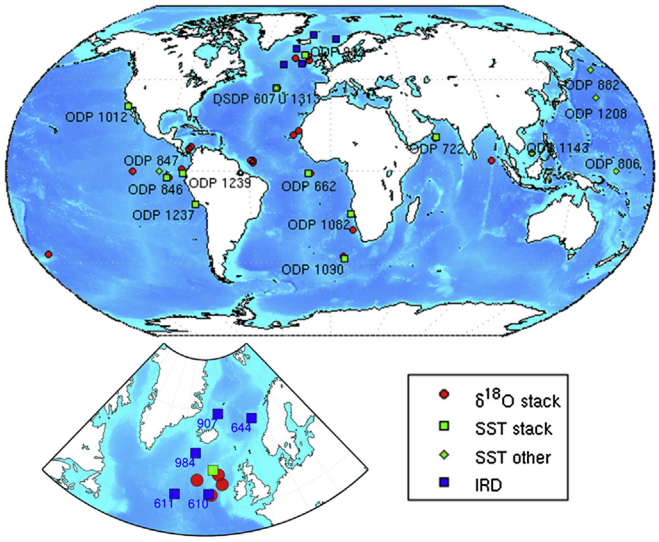

Fig. 4. Map of the source locations of the data used in this study: $\delta^{18}O$ cores from the (Lisiecki and Raymo, 2005) stack in red (22 sites in total), sea surface temperatures (SSTs) in green (16 sites; squares represent all 10 sites entering the Martínez-Botí et al. (2015) global stack and include data from Lawrence et al. (2006, 2009), Dekens et al. (2007), Etourneau et al. (2009, 2010), Brierley et al. (2009), Herbert et al. (2010), Lawrence and Chase (2010), Martínez-Garcia et al. (2010) and Naafs et al. (2012); diamonds represent the sites of other SST reconstructions from Medina-Elizalde et al. (2008), Naafs et al. (2010), Li et al. (2011) and Venti et al. (2013) and ice rafted debris (IRDs) in blue (5 sites). (For interpretation of the references to colour in this figure legend, the reader is referred to the web version of this article.)

contribution was around 10% (e.g. DeConto et al., 2012) and AIS volume changes were primarily driven by sea level variations caused by the NH ice sheets. When assuming the same ratio for the earlier Pleistocene, additional 0.1‰ of uncertainties is introduced. This, however, is a rather conservative estimate since modelling results (Pollard and DeConto, 2009; de Boer et al., 2014) suggest smaller magnitude of Antarctic ice volume variability. Therefore, although the Antarctic ice sheet contribution to $\delta^{18}O$ is not negligible, it is likely to be significantly smaller than the averaged $\delta^{18}O$ trend across the PPT of 0.7‰/My and the magnitude of early Pleistocene $\delta^{18}O$ cycles (ca 1‰). For this end and due to absence of reliable empirical or modelling data we neglected the AIS contribution to $\delta^{18}O$ and only considered NH contribution.

The model equivalent of the $\delta^{18}O$ stack is computed by averaging the $\delta^{18}O$ values computed from the annual mean deep-sea temperature in the ocean basin and latitudinal band corresponding to each single core and then averaging over all cores.

A quantitative and objective selection of the best CO_2 scenarios is based on a combination of a Taylor score and a trend score for both $\delta^{18}O$ and global SST. The Taylor score (Taylor, 2001) takes into account the correlation (R) between model and data, the ratio of the standard deviation of the modelled quantity relative to the data ($\sigma = \sigma_{model}/\sigma_{data}$) and implicitly the root mean square error of the model and combines this information into a single number:

$$S_{Taylor} = \frac{4(1+R)^4}{\left(\sigma + \frac{1}{\sigma}\right)^2 (1+R_0)^4},$$

where R_0 is the maximum model-data correlation which can be attained and is taken to be $R_0 = 1$.

The trend score is computed as (Dalmonech and Zaehle, 2013):

$$S_{trend} = \frac{1}{\left(1 + \left|\frac{trend_{data} - trend_{model}}{trend_{data}}\right|\right)^2}.$$

S_{trend} has the property of being symmetric, with a value of 1 if the observed and modelled trends match and decays rapidly as the observed and modelled trends diverge.

The S_{Taylor} and S_{trend} scores are then normalized between 0 and 1 and combined to give an overall measure of the model-data agreement as follows:

$$S = \frac{S_{Taylor}\left(\delta^{18}O\right) + S_{Taylor}(SST) + S_{trend}\left(\delta^{18}O\right) + S_{trend}(SST)}{4}.$$

S gives equal weight to measures of climate variability and long term trends.

Finally, a ranking of the score S of the ensemble model simulations with different CO_2 scenarios allows determination of the best CO_2 scenarios given the constraints on $\delta^{18}O$ and SST variability and trends.

3. Results and discussion

3.1. Selection of the best CO_2 scenarios

The ensemble members with the best score S are generally in very good agreement with the LR04 stack (Fig. 5). The match between modelled and reconstructed SSTs is generally less good, but model and data agree reasonably well after 2.7 Ma (Fig. 6). The model is able to closely reproduce the long-term trends in $\delta^{18}O$ and SST (Fig. 7). The simulation with the CO_2 scenario constrained only by the Taylor scores overestimates the magnitude of the trends in both $\delta^{18}O$ and SSTs (Fig. 7). Combining the constraint on $\delta^{18}O$ and SST variability with the constraint on trends results in modelled trends that are very close to the observations (Fig. 7). The information from variability and long-term trends are therefore not redundant and if combined provide a better constraint on the CO_2 scenario.

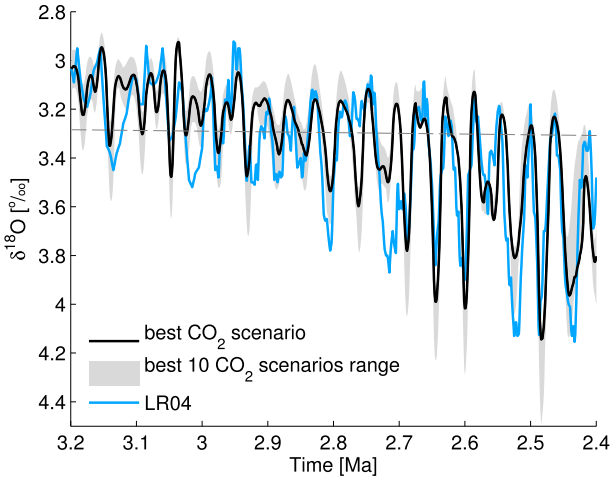

Fig. 5. Benthic $\delta^{18}O$ over the time interval 3.2–2.4 Ma. Model derived $\delta^{18}O$ for the best CO_2 scenario (solid black) with shading representing the range covered by the best ten CO_2 scenarios. The (Lisiecki and Raymo, 2005) stack is shown for comparison (blue). The horizontal dashed line indicates the present day LR04 $\delta^{18}O$ value of 3.23‰. (For interpretation of the references to colour in this figure legend, the reader is referred to the web version of this article.)

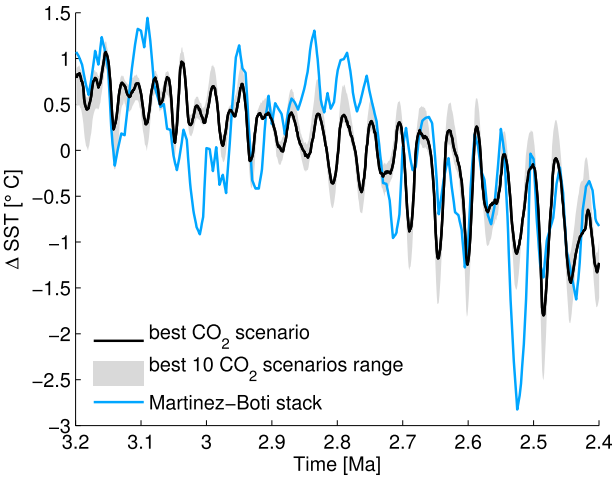

Fig. 6. Relative global sea surface temperature variations over the time interval 3.2–2.4 Ma. Modelled global annual sea surface temperature for the best CO_2 scenario (solid black) with shading representing the range covered by the best ten CO_2 scenarios. The (Martínez-Botí et al., 2015) global SST stack is shown for comparison (blue). (For interpretation of the references to colour in this figure legend, the reader is referred to the web version of this article.)

3.2. Best CO_2 scenarios

Our constrained model results are consistent with a gradual CO_2 decrease ranging from 100 to 125 ppm in the interval between 3.2 and 2.4 Ma (Fig. 8). The estimates of the CO_2 concentration at 3.2 Ma for the best ten scenarios determined by the S score range from 375 to 425 ppm and the CO_2 drops to values between 275 and

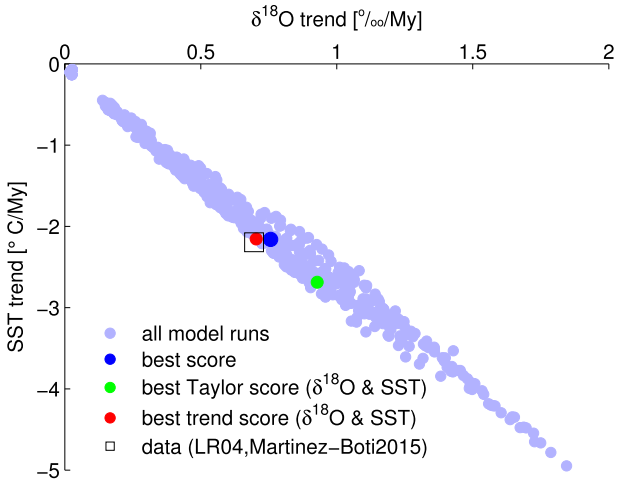

Fig. 7. Scatterplot of global SST and $\delta^{18}O$ trends over the time interval 3.2–2.4 Ma. All model runs (540) are shown in light blue. The simulation with the CO_2 scenario which gives the best score S (dark blue), the one with the best Taylor score for $\delta^{18}O$ and SST (green) and the one with the best trend score (red) are also shown. Data are represented by the LR04 stack (Lisiecki and Raymo, 2005) and by the global SST stack of Martínez-Botí et al. (2015). (For interpretation of the references to colour in this figure legend, the reader is referred to the web version of this article.)

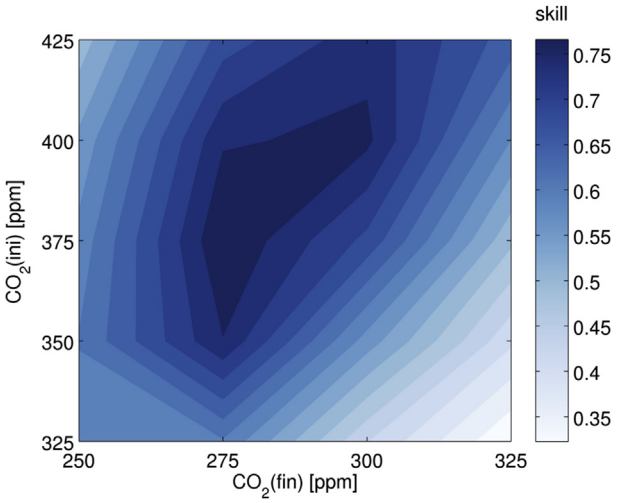

Fig. 9. Total model skill (S) as a function of the initial and final CO_2 concentrations in the idealized CO_2 scenarios.

300 ppm at 2.4 Ma. The final CO_2 concentration is very tightly constrained by our simulations, better than the late Pliocene value (Fig. 9). The model-based estimates of the CO_2 evolution during the PPT are consistent with a long-term CO_2 decline seen also in the reconstructions by Seki et al. (2010) and Martínez-Botí et al. (2015). All best CO_2 scenarios are characterized by a pronounced orbital-scale variability represented here in terms of an obliquity component, i.e. 20–40 ppm CO_2 change per one degree of obliquity change. However, the range of CO_2 variability in the scenarios is lower than suggested by the reconstructions of Bartoli et al. (2011) and Martínez-Botí et al. (2015) (Figs. 1 and 8). It is unclear however whether the spread of CO_2 concentrations in the reconstructions represents orbital-scale variability of CO_2 or just uncertainties of the method.

Having determined plausible CO_2 scenarios for the whole period from 3.2 to 2.4 Ma we use the corresponding CLIMBER-2 simulations to model the evolution of NH ice sheets and global climate according to the steps 2–4 outlined in Section 2.3. The results are presented in the next sections.

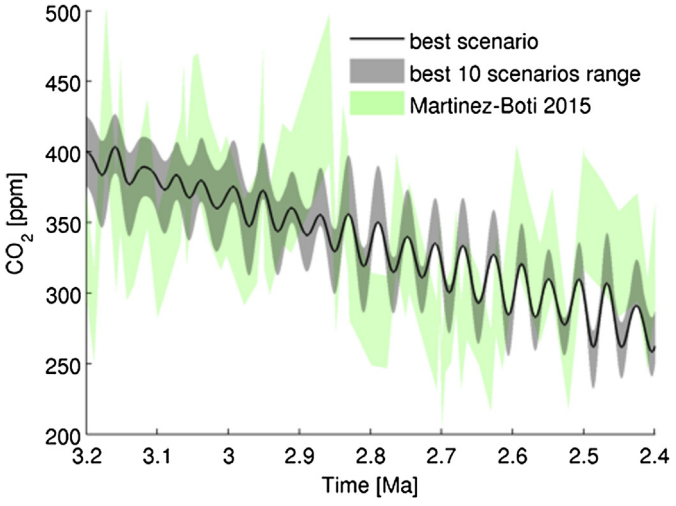

Fig. 8. The best CO_2 scenario resulting from our 'inverse' modelling approach (solid black line) and the range of the best ten CO_2 scenarios (grey shading) compared to the most recent high resolution CO_2 reconstruction from Martínez-Botí et al. (2015).

3.3. Intensification of Northern Hemisphere glaciation

The increase in mean values and variability of benthic $\delta^{18}O$ through the PPT provides strong evidence for deep ocean cooling, an increase in global ice volume and an increasingly stronger response of the Earth system to orbital forcing (Mudelsee and Raymo, 2005; Sosdian and Rosenthal, 2009; Miller et al., 2012). All these changes in climate variability across the PPT are well captured by our model simulations driven by the best CO_2 scenarios (Fig. 5). Interestingly, the major discrepancies in $\delta^{18}O$ between model and data are observed between 2.8 and 2.7 Ma (Fig. 5). The modelled increase in $\delta^{18}O$ corresponding to the minimum in June insolation at around 2.77 Ma has no counterpart in the data, while the subsequent strong increase in the LR04 stack after 2.74 Ma is much weaker in the model. The occurrence of these discrepancies roughly corresponds to the time period when the North Pacific stratification is thought to have increased, around 2.73 Ma (Haug et al., 2005; Studer et al., 2012). Without applying additional forcings to the model no substantial changes in the North Pacific region occur during the simulation interval. This might partly explain the model-data differences. A recent sea level reconstruction by Rohling et al. (2014) suggests that the increase in $\delta^{18}O$ at around 2.73 Ma was mainly caused by a deep ocean temperature signal, rather than being associated with an increase in ice volume. This deep ocean temperature signal could be related to the circulation change and heat transport idea put forth in a recent study by Woodard et al. (2014), which suggests a shift to stronger heat transfer from the North Atlantic to the Deep Pacific around this time. This would imply that for the specific interval of time our generic CO_2 scenario is not accurate enough.

The model simulates a general increase in NH ice volume during glacials from 3.2 to 2.4 Ma, while over the same period no significant changes in ice volume are modelled during interglacials, in agreement with proxy data (Fig. 10a). The most significant glaciation events occur rather abruptly after 2.7 Ma during periods of minimum summer and annual insolation, i.e. during periods of low obliquity, and low CO_2, since the latter is linearly related to obliquity (Fig. 10a). Precession also plays a role but obliquity dominates.

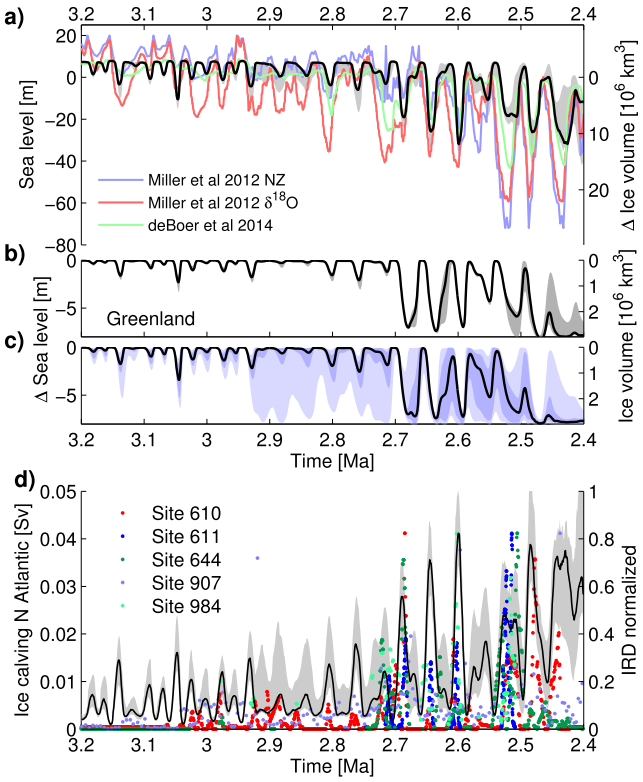

Fig. 10. (a) Modelled NH ice volume and sea level equivalent (black line and shading representing the median and range of the combination of the simulations with the ten best CO_2 scenarios and the Greenland ensemble) compared to sea level reconstructions. Reconstructions include $\delta^{18}O$ scaled to sea level (red, (Miller et al., 2012)), conversion of benthic $\delta^{18}O$ with support from New Zealand sequence stratigraphic data (blue, (Naish and Wilson, 2009; Miller et al., 2012)) and estimates from a model-based deconvolution of benthic $\delta^{18}O$ (green, (de Boer et al., 2014b)). (b,c) Modelled Greenland ice volume and equivalent sea level change. The grey shading in (b) represents the range from the best ten CO_2 scenarios while the blue shading in (c) represents the different model parameter choices in REMBO-SICOPOLIS (light blue indicates the model range and dark blue the interquantile range). (d) Modelled calving into the North Atlantic (solid black line with shading) compared to ice rafted debris (IRDs) as recorded in various marine cores in the North Atlantic (sites indicated in Fig. 4); DSDP Site 610 (Flesche Kleiven et al., 2002), DSDP Site 611 (Bailey et al., 2013), ODP Site 644 (Jansen and Sjøholm, 1991), ODP Site 907 (Jansen et al., 2000) and ODP Site 984 (Bartoli et al., 2006). All IRD data are normalized to their maximum value and plotted scaled to the maximum calving in the model. Modelled calving is smoothed with a 1000 year window. (For interpretation of the references to colour in this figure legend, the reader is referred to the web version of this article.)

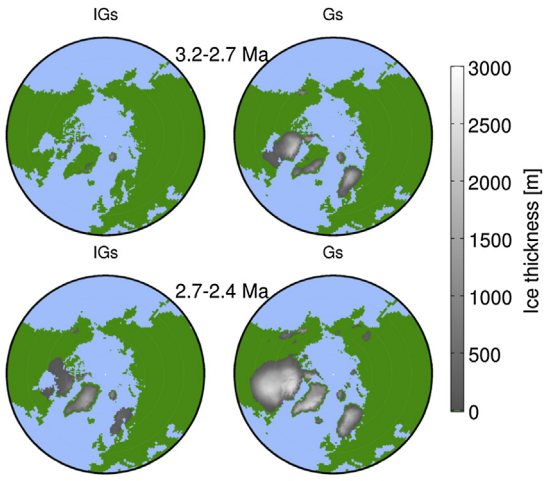

Fig. 11. Mean ice thickness during interglacials (left) and glacials (right) for the interval 3.2–2.7 Ma (top) and for the interval 2.7–2.4 Ma (bottom). Shown is the ENS_CLIM ensemble mean ice thickness for continental ice sheets and the ENS_GRL ensemble mean for the Greenland ice sheet.

The same is true also for the simulated Greenland ice sheet volume, although Greenland shows an even more abrupt transition to full glaciation after 2.7 Ma (Fig. 10b). The full Greenland glaciation as a response to a CO_2 drop of around 100 ppm is consistent with the results from Lunt et al. (2008), which suggested that a CO_2 decrease was the fundamental driver of Greenland glaciation.

The maximum NH ice volume during the simulation period is equivalent to a drop in sea level by around 40 m, from which 7 m are attributable to the full Greenland glaciation (Fig. 10a,b).

During the time interval 3.2–2.7 Ma, the NH is essentially ice free most of the time. During 'glacials', ice sheets cover northern Scandinavia, southeast Greenland and parts of northern Canada (Fig. 11). In the interval from 2.7 to 2.4 Ma the NH continents are still almost ice-free during interglacials but become significantly glaciated during glacial maxima, when Scandinavia is fully ice covered and a large ice sheet appears over North America (Fig. 11). On average after 2.7 Ma Greenland is almost completely ice covered, although the ice sheet is significantly thinner during interglacials compared to glacial periods (Fig. 11).

Changes in sea-level equivalent are also compared to sea level reconstructions in Fig. 10. There is a wide spread in both absolute values and variability of the reconstructions (Naish and Wilson, 2009; Miller et al., 2012; de Boer et al., 2014b). Maximum sea level during the Pliocene is estimated to be around 25 m higher than today (Dwyer and Chandler, 2009; Miller et al., 2012), although estimates vary widely between +10 and +60 m among studies (Dowsett and Cronin, 1990; Krantz, 1991; Wardlaw and Quinn, 1991; Kaufman and Brigham-Grette, 1993; James et al., 2006) and estimates based on paleo-shoreline reconstructions could be affected by glacial isostatic adjustment (Raymo et al., 2011) and/or dynamic topography changes (Rowley et al., 2013). It is important to realize that the maximum contribution from the NH to sea level rise relative to present day is quantified as 7 m from Greenland melt. An additional 5 m would come from a collapse of West Antarctica, which has been shown to be sensitive to orbital forcing throughout the Pliocene (Pollard and DeConto, 2009). Therefore, sea level higher than +12 m above present day level would require a substantial contribution from East Antarctica. Since Antarctica is prescribed to its present day volume in our model, our maximum Pliocene sea level is 7 m higher than present as it accounts only for the melted GrIS. Additionally, if Antarctica was indeed more sensitive to orbital forcing than it was during the last million years (Williams et al., 2010; Cook et al., 2013), we may also underestimate sea level variability in our simulations, since our model does not include an interactive Antarctic ice sheet. The amplitude of sea level variations in the model is roughly consistent with reconstructions, except for after 2.55 Ma, when the model seems to underestimate ice volume increases during glacial maxima.

An intensification of the Northern Hemisphere glaciation at around 2.7 Ma is also confirmed by the appearance of ice rafted debris recorded at several locations in the North Atlantic and North Sea (Fig. 4). IRDs are qualitatively compared with modelled ice calving into the North Atlantic in Fig. 10d. A significant and relatively abrupt increase in the IRD content in marine sediments is evident at around 2.7 Ma and is qualitatively in agreement with a modelled increase in ice calving from the Greenland, Fennoscandian and Laurentide ice sheets at that time. The modelled calving peaks during glacial maxima after 2.7 Ma all have corresponding peaks in observed IRDs.

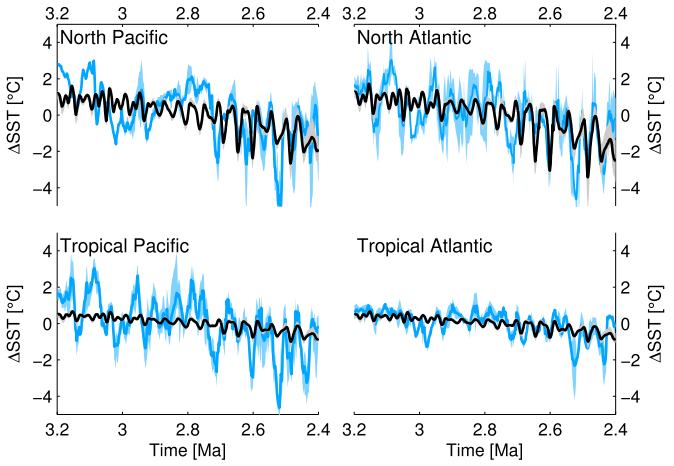

Fig. 12. Time series of modelled (black) and reconstructed (blue) SST anomalies over the four regions as indicated in the panels. The reconstructed SSTs represent the mean (solid line) and range (shading) of all the reconstructions from sites falling into the respective region (North Pacific: ODP 1012 (Brierley et al., 2009), ODP 1208 (Venti et al., 2013); North Atlantic: ODP 982 (Lawrence et al., 2009), DSDP 607 (Lawrence et al., 2010), U 1313 (Naafs et al., 2010); Tropical Pacific: ODP 846 (Lawrence et al., 2006), ODP 806 (Medina-Elizalde et al., 2008), ODP 847 (Dekens et al., 2007), ODP 1143 (Li et al., 2011), ODP 1237 (Dekens et al., 2007), ODP 1239 (Etourneau et al., 2010); Tropical Atlantic: ODP 622 (Herbert et al., 2010), ODP 1082 (Etourneau et al., 2009)). (For interpretation of the references to colour in this figure legend, the reader is referred to the web version of this article.)

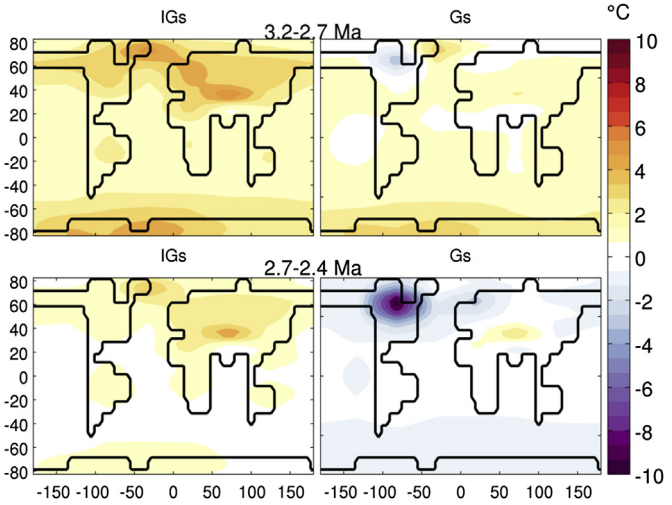

Fig. 13. June–July–August (JJA) surface air temperature anomalies relative to preindustrial during interglacials (left) and glacials (right) for the interval 3.2–2.7 Ma (top) and for the interval 2.7–2.4 Ma (bottom). Shown is the ENS_CLIM ensemble mean temperature.

3.4. Climate evolution

While benthic $\delta^{18}O$ reconstructions represent an integrated global signal of ice volume and deep ocean temperature, SST reconstructions are representative of much more local conditions. This makes a direct comparison of modelled and reconstructed SSTs less straightforward, in particular considering the relatively low resolution of the ocean model employed in this study. SSTs can be strongly influenced by local circulation changes, which are hardly captured by a zonally averaged ocean model. In Fig. 12 modelled SSTs are compared to reconstructions in the North Pacific, the North Atlantic, the Tropical Pacific and the Tropical Atlantic. The model captures the long term cooling over all regions and most of the variability in the high latitudes after ~2.7 Ma. In general there is notably more variability in the reconstructed than in the modelled SSTs in all regions, but particularly in the Tropical Pacific. This could be related to changes in zonal Pacific SST variations which are not resolved by the model. A rapid cooling event at around 2.75 Ma is probably the most prominent feature consistent in all datasets with no counterpart in the model and might be related to some reorganization of the ocean circulation (like onset of the North Pacific stratification (Sigman et al., 2004)) or increase of interhemispheric heat transport (Woodard et al., 2014), which is not reproduced by the model, or to an inadequate CO_2 scenario for this time interval. Although the model does not capture all the variability in the SSTs, as already shown above, it performs reasonably well at reproducing the long term cooling.

Summer surface air temperatures together with summer insolation control the amount of ice that can be melted during the warm season and therefore are important for the evolution of ice sheets. During interglacials before 2.7 Ma summer temperatures are everywhere higher than preindustrial (Fig. 13). The warming is particularly pronounced over the NH continents and over Antarctica with temperatures more than 5 °C warmer. During glacials, summers are locally cooler than preindustrial over northern North America and over northern Europe, ie., regions covered by small ice sheets (Figs. 11 and 13). After 2.7 Ma, summer temperatures are only locally warmer than preindustrial during interglacials, particularly over the shallower Greenland ice sheet (Figs. 13 and 11). During glacials, summer temperatures are significantly colder than preindustrial over most NH boreal areas, especially over the region covered by the thick Laurentide ice sheet where temperatures are up to 10 °C lower (Fig. 13).

3.5. Response to different components of orbital forcing

Variations in orbital configuration play a fundamental role in controlling glaciation on Earth. It is generally believed that summer insolation determines the glaciation periods. The classical Milankovic theory (Milankovic, 1941) is based on an assumption that NH ice sheets are sensitive to the boreal summer insolation. During the time interval covered by our simulations, benthic foraminifera $\delta^{18}O$ shows an increased response to the obliquity forcing going from 3.2 to 2.4 Ma (Lisiecki and Raymo, 2007), while the precessional component remains small (Fig. 14a). This shows that the climate-ice sheet system responded mostly to obliquity changes, which may in part be due to the fact that obliquity controls the rate of heat exchange between the low and high latitudes (Raymo and Nisancioglu, 2003). An alternative theory for the dominance of the obliquity signal in the LR04 stack is based on the assumption that ice volume changes occurred in both the Northern and Southern Hemispheres, controlled by local summer insolation (Raymo et al., 2006). Since precession-induced insolation variations are out of phase between NH and SH, the changes in ice volume between the two hemispheres could balance out resulting in a small global response to precession, leaving only the obliquity signal in globally integrated measures like benthic $\delta^{18}O$.

Results of our simulations suggest that a strong response of the Antarctic ice sheet to local precessional forcing is not required to explain the dominance of the obliquity signal in benthic $\delta^{18}O$. Our model simulates only a weak response of NH ice volume and $\delta^{18}O$ in the precessional band (periods around 20 kyr, Fig. 14a,b), similar to what is found in data. Modelled and reconstructed sea level and $\delta^{18}O$ are dominated by variability at frequencies corresponding to obliquity variations (Fig. 14a,b). This implies that the NH ice sheets responded predominantly to obliquity. Similarly, modelling studies of the Antarctic ice sheet found that the West Antarctic Ice

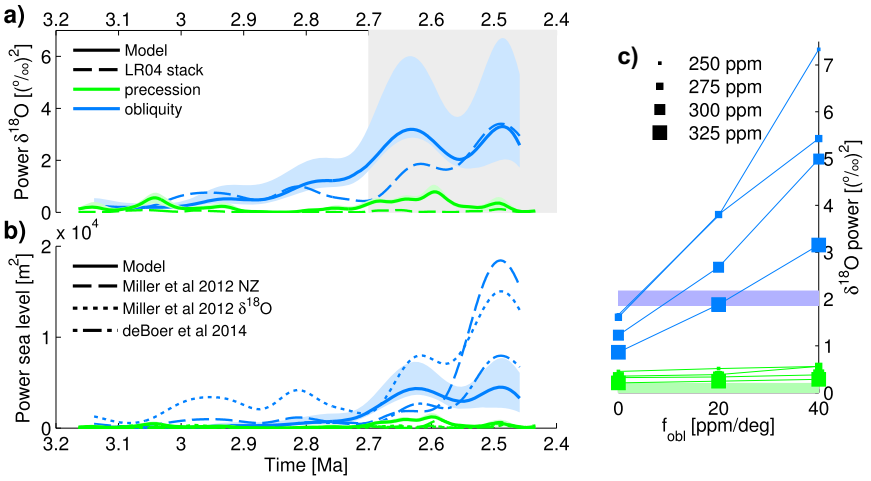

Fig. 14. Left: $\delta^{18}O$ (a) and sea level (b) power in the frequency bands corresponding to variations in obliquity (37–44 kyr, blue) and precession (18–25 kyr, green). Solid lines with shading represent the model (median and range of the ENS_CLIM/ENS_GRL ensemble) while other line styles represent different data sources as indicated in the legends. (c) Mean $\delta^{18}O$ power in the time interval 2.7–2.4 Ma (interval highlighted by the grey shading in (a)) in the frequency bands corresponding to obliquity (blue) and precession (green) variations as a function of the obliquity factor (f_{obl} in eq. (1)) in the CO_2 scenarios. The size of the symbols represents different final CO_2 concentrations (CO_2(fin) in eq. (1)) as shown in the legend. Reference values derived from the Lisiecki and Raymo (2005) benthic $\delta^{18}O$ stack are shown as shaded horizontal bars. Power is computed from a time-frequency wavelet spectrum. (For interpretation of the references to colour in this figure legend, the reader is referred to the web version of this article.)

sheet also responded mostly to obliquity forcing during the Pliocene and early Pleistocene (Naish et al., 2009). The best CO_2 scenarios derived above and used to force the model all have an obliquity component, which might suppress the model response to precession and amplify the response to obliquity. However, the obliquity response is also dominant in simulations without an obliquity component in the CO_2 scenario as shown in Fig. 14c. The CO_2 obliquity component only acts to further amplify the system's response at the 41 kyr period, but does not affect the amplitude of the model response to precession (Fig. 14c).

The climate-ice sheet response at the frequency of obliquity variations increases through time from 3.2 to 2.4 Ma (Fig. 14a,b), corresponding to an increase in the power of the forcing at 41 kyr (Fig. 3) and increase in magnitude of NH ice volume variations.

4. Conclusions

In this paper we presented a novel model-based approach to reconstructing plausible CO_2 scenarios that accompanied the Pliocene–Pleistocene transition. A linear CO_2 decrease by about 100 ppm, from 375–425 ppm at 3.2 Ma to 275–300 ppm at 2.4 Ma, with an additional obliquity component of 40–60 ppm gives the best model agreement with $\delta^{18}O$ and global SST reconstructions. Our simulated CO_2 decrease of 100–125 ppm is consistent with some recent data based estimates (Seki et al., 2010; Martínez-Botí et al., 2015), which provides additional support for our findings.

The model forced with the best CO_2 scenarios shows a relatively abrupt intensification of NH glaciation at around 2.7 Ma. While before 2.7 Ma, glacial maxima where characterized by limited ice sheet extents over parts of Greenland, Scandinavia and Northern Canada, major ice sheets only covered North America, all of Greenland and Scandinavia during glacial maxima after 2.7 Ma. Greenland shows a particularly abrupt transition from partly to fully glaciated conditions at around 2.7 Ma. Our results are supported by evidence of an increase in ice rafted debris deposited in marine sediments at various locations in the North Atlantic and the North Sea after 2.7 Ma. The modelled equivalent sea-level variations are also broadly consistent with the wide range of estimates from data, except for the period after 2.55 Ma when the model seems to underestimate ice volume variability. It is however important to note that our model simulates ice sheets only in the Northern Hemisphere.

The increasing dominance of the 41 kyr obliquity response in the model is in qualitative agreement with the observed response in benthic $\delta^{18}O$, sea level and SST reconstructions. The modelled response to precession is generally small and consistent with estimates from data. The strong obliquity response has already been seen in simulations with constant CO_2 (Ganopolski and Calov, 2011). In the case of our best CO_2 scenarios, the obliquity component in ice volume and climate response is additionally amplified by the obliquity component in the prescribed CO_2 scenarios.

Acknowledgements

M.W. acknowledges support by the German Science Foundation DFG grant GA 1202/2-1. A.R. was funded by the Marie Curie 7th Framework Programme (Project PIEF-GA-2012-331835, EURICE). The comments of two anonymous reviewers helped to improve the paper.

References

Abe-Ouchi, A., Saito, F., Kawamura, K., Raymo, M.E., Okuno, J., Takahashi, K., Blatter, H., 2013. Insolation-driven 100,000-year glacial cycles and hysteresis of ice-sheet volume. Nature 500, 190–193. http://dx.doi.org/10.1038/nature12374.

Archer, D., Martin, P., Buffett, B., Brovkin, V., Rahmstorf, S., Ganopolski, A., 2004. The importance of ocean temperature to global biogeochemistry. Earth Planet. Sci. Lett. 222, 333–348. http://dx.doi.org/10.1016/j.epsl.2004.03.011.

Badger, M.P.S., Schmidt, D.N., Mackensen, A., Pancost, R.D., 2013. High-resolution alkenone palaeobarometry indicates relatively stable pCO(2) during the Pliocene (3.3-2.8 Ma). Philos. Trans. A. Math. Phys. Eng. Sci. 371, 20130094. http://dx.doi.org/10.1098/rsta.2013.0094.

Bailey, I., Hole, G.M., Foster, G.L., Wilson, P.A., Storey, C.D., Trueman, C.N., Raymo, M.E., 2013. An alternative suggestion for the Pliocene onset of major northern hemisphere glaciation based on the geochemical provenance of North Atlantic Ocean ice-rafted debris. Quat. Sci. Rev. 75, 181–194. http://dx.doi.org/10.1016/j.quascirev.2013.06.004.

Barreiro, M., Philander, G., Pacanowski, R., Fedorov, A., 2005. Simulations of warm tropical conditions with application to middle Pliocene atmospheres. Clim. Dyn. 26, 349–365. http://dx.doi.org/10.1007/s00382-005-0086-4.

Bartoli, G., Sarnthein, M., Weinelt, M., Erlenkeuser, H., Garbe-Schönberg, D., Lea, D.W., 2005. Final closure of Panama and the onset of northern hemisphere glaciation. Earth Planet. Sci. Lett. 237, 33–44. http://dx.doi.org/10.1016/j.epsl.2005.06.020.

Bartoli, G., Sarnthein, M., Weinelt, M., 2006. Late Pliocene millennial-scale climate variability in the northern North Atlantic prior to and after the onset of

Northern Hemisphere glaciation. Paleoceanography 21. http://dx.doi.org/10.1029/2005PA001185.
Bartoli, G., Hönisch, B., Zeebe, R.E., 2011. Atmospheric CO_2 decline during the Pliocene intensification of Northern Hemisphere glaciations. Paleoceanography 26, 1–14. http://dx.doi.org/10.1029/2010PA002055.
Berger, A., Loutre, M.F., 1992. Astronomical solutions for paleoclimate studies over the last 3 million years. Earth Planet. Sci. Lett. 111, 369–382. http://dx.doi.org/10.1016/0012-821X(92)90190-7.
Berger, W.H., Wefer, G., 1996. Expeditions into the Past: paleoceanographic studies in the South Atlantic. In: Wefer, G., Berger, W.H., Siedler, G., Webb, D.J. (Eds.), The South Atlantic: Present and Past Circulation. Springer Berlin Heidelberg, Berlin, Heidelberg, pp. 363–410. http://dx.doi.org/10.1007/978-3-642-80353-6.
Berger, W., Bickert, T., Schmidt, H., Wefer, G., Yasuda, M., 1993. Quaternary oxygen isotope record of pelagic foraminifers: site 805, Ontong Java Plateau. Proc. Ocean. Drill. Program, Sci. Results 130, 363–379.
Berger, A., Li, X.S., Loutre, M.F., 1999. Modelling northern hemisphere ice volume over the last 3 Ma. Quat. Sci. Rev. 18, 1–11. http://dx.doi.org/10.1016/S0277-3791(98)00033-X.
Boos, W.R., Kuang, Z., 2010. Dominant control of the South Asian monsoon by orographic insulation versus plateau heating. Nature 463, 218–222. http://dx.doi.org/10.1038/nature08707.
Brierley, C.M., Fedorov, A.V., 2010. Relative importance of meridional and zonal sea surface temperature gradients for the onset of the ice ages and Pliocene-Pleistocene climate evolution. Paleoceanography 25, PA2214. http://dx.doi.org/10.1029/2009PA001809.
Brierley, C.M., Fedorov, A.V., Liu, Z., Herbert, T.D., Lawrence, K.T., Lariviere, J.P., 2009. Greatly expanded tropical warm pool and weakened Hadley circulation in the early Pliocene. Science 323, 1714–1718. http://dx.doi.org/10.1126/science.1167625.
Brovkin, V., Ganopolski, A., Svirezhev, Y., 1997. A continuous climate-vegetation classification for use in climate-biosphere studies. Ecol. Modell. 101, 251–261.
Brovkin, V., Bendtsen, J., Claussen, M., Ganopolski, A., Kubatzki, C., Petoukhov, V., Andreev, A., 2002. Carbon cycle, vegetation, and climate dynamics in the Holocene: experiments with the CLIMBER-2 model. Glob. Biogeochem. Cycles 16 (4), 1139. http://dx.doi.org/10.1029/2001GB001662.
Brovkin, V., Ganopolski, A., Archer, D., Rahmstorf, S., 2007. Lowering of glacial atmospheric CO_2 in response to changes in oceanic circulation and marine biogeochemistry. Paleoceanography 22. http://dx.doi.org/10.1029/2006PA001380 n/a–n/a.
Brovkin, V., Ganopolski, a., Archer, D., Munhoven, G., 2012. Glacial CO_2 cycle as a succession of key physical and biogeochemical processes. Clim. Past 8, 251–264. http://dx.doi.org/10.5194/cp-8-251-2012.
Burton, K.W., Ling, H.-F., O'Nions, R.K., 1997. Closure of the Central American Isthmus and its effect on deep-water formation in the North Atlantic. Nature 386, 382–385. http://dx.doi.org/10.1038/386382a0.
Calov, R., Ganopolski, A., 2005. Multistability and hysteresis in the climate-cryosphere system under orbital forcing. Geophys. Res. Lett. 32, L21717. http://dx.doi.org/10.1029/2005GL024518.
Calov, R., Ganopolski, A., Claussen, M., Petoukhov, V., Greve, R., 2005. Transient simulation of the last glacial inception. Part I: glacial inception as a bifurcation in the climate system. Clim. Dyn. 24, 545–561. http://dx.doi.org/10.1007/s00382-005-0007-6.
Calov, R., Robinson, A., Perrette, M., Ganopolski, A., 2015. Simulating the Greenland ice sheet under present-day and palaeo constraints including a new discharge parameterization. Cryosph. 9, 179–196. http://dx.doi.org/10.5194/tc-9-179-2015.
Cane, M.A., Molnar, P., 2001. Closing of the Indonesian seaway as a precursor to east African aridification around 3–4 million years ago. Nature 411, 157–162. http://dx.doi.org/10.1038/35075500.
Cook, C.P., van de Flierdt, T., Williams, T., Hemming, S.R., Iwai, M., Kobayashi, M., Jimenez-Espejo, F.J., Escutia, C., González, J.J., Khim, B.-K., McKay, R.M., Passchier, S., Bohaty, S.M., Riesselman, C.R., Tauxe, L., Sugisaki, S., Galindo, A.L., Patterson, M.O., Sangiorgi, F., Pierce, E.L., Brinkhuis, H., Klaus, A., Fehr, A., Bendle, J.A.P., Bijl, P.K., Carr, S.A., Dunbar, R.B., Flores, J.A., Hayden, T.G., Katsuki, K., Kong, G.S., Nakai, M., Olney, M.P., Pekar, S.F., Pross, J., Röhl, U., Sakai, T., Shrivastava, P.K., Stickley, C.E., Tuo, S., Welsh, K., Yamane, M., 2013. Dynamic behaviour of the East Antarctic ice sheet during Pliocene warmth. Nat. Geosci. 6, 765–769. http://dx.doi.org/10.1038/ngeo1889.
Copeland, P., Mark Harrison, T., Kidd, W.S.F., 1987. Rapid early Miocene acceleration of uplift in the Gangdese Belt, Xizang (southern Tibet), and its bearing on accommodation mechanisms of the India-Asia collision. Earth Planet. Sci. Lett. 86, 240–252. http://dx.doi.org/10.1016/0012-821X(87)90224-X.
Crowley, T.J., Baum, S.K., 1995. Reconciling Late Ordovician (440 Ma) glaciation with very high (14X) CO_2 levels. J. Geophys. Res. 100, 1093. http://dx.doi.org/10.1029/94JD02521.
Dalmonech, D., Zaehle, S., 2013. Towards a more objective evaluation of modelled land-carbon trends using atmospheric CO_2 and satellite-based vegetation activity observations. Biogeosciences 10, 4189–4210. http://dx.doi.org/10.5194/bg-10-4189-2013.
De Boer, B., van de Wal, R.S.W., Lourens, L.J., Bintanja, R., 2012. Transient nature of the Earth's climate and the implications for the interpretation of benthic records. Palaeogeogr. Palaeoclimatol. Palaeoecol. 335–336, 4–11. http://dx.doi.org/10.1016/j.palaeo.2011.02.001.
De Boer, B., Lourens, L.J., van de Wal, R.S.W., 2014. Persistent 400,000-year variability of Antarctic ice volume and the carbon cycle is revealed throughout the Plio-Pleistocene. Nat. Commun. 5, 2999. http://dx.doi.org/10.1038/ncomms3999.
DeConto, R.M., Pollard, D., Kowalewski, D., 2012. Modeling Antarctic ice sheet and climate variations during Marine Isotope Stage 31. Glob. Planet. Change 88–89, 45–52. http://dx.doi.org/10.1016/j.gloplacha.2012.03.003.
Dekens, P.S., Ravelo, A.C., McCarthy, M.D., 2007. Warm upwelling regions in the Pliocene warm period. Paleoceanography 22. http://dx.doi.org/10.1029/2006PA001394 n/a–n/a.
Dolan, A.M., Haywood, A.M., Hill, D.J., Dowsett, H.J., Hunter, S.J., Lunt, D.J., Pickering, S.J., 2011. Sensitivity of Pliocene ice sheets to orbital forcing. Palaeogeogr. Palaeoclimatol. Palaeoecol. 309, 98–110. http://dx.doi.org/10.1016/j.palaeo.2011.03.030.
Dolan, A.M., Hunter, S.J., Hill, D.J., Haywood, A.M., Koenig, S.J., Otto-Bliesner, B.L., Abe-Ouchi, A., Bragg, F., Chan, W.-L., Chandler, M.A., Contoux, C., Jost, A., Kamae, Y., Lohmann, G., Lunt, D.J., Ramstein, G., Rosenbloom, N.A., Sohl, L., Stepanek, C., Ueda, H., Yan, Q., Zhang, Z., 2015. Using results from the PlioMIP ensemble to investigate the Greenland Ice Sheet during the mid-Pliocene Warm Period. Clim. Past 11, 403–424. http://dx.doi.org/10.5194/cp-11-403-2015.
Dowsett, H.J., Cronin, T.M., 1990. High Eustatic sea level during the middle Pliocene: Evidence from the southeastern U.S. Atlantic Coastal Plain. Geology 18, 435–438. http://dx.doi.org/10.1130/0091-7613(1990)018.
Dwyer, G.S., Chandler, M.A., 2009. Mid-Pliocene sea level and continental ice volume based on coupled benthic Mg/Ca palaeotemperatures and oxygen isotopes. Philos. Trans. A. Math. Phys. Eng. Sci. 367, 157–168. http://dx.doi.org/10.1098/rsta.2008.0222.
Einarsson, T., Hopkins, D.M., Doell, R., 1967. The Stratigraphy of Tjörnes, Northern Iceland, and the History of the Bering Land Bridge.
Etourneau, J., Martinez, P., Blanz, T., Schneider, R., 2009. Pliocene-Pleistocene variability of upwelling activity, productivity, and nutrient cycling in the Benguela region. Geology 37, 871–874. http://dx.doi.org/10.1130/G25733A.1.
Etourneau, J., Schneider, R., Blanz, T., Martinez, P., 2010. Intensification of the Walker and Hadley atmospheric circulations during the Pliocene–Pleistocene climate transition. Earth Planet. Sci. Lett. 297, 103–110. http://dx.doi.org/10.1016/j.epsl.2010.06.010.
Fedorov, A.V., Brierley, C.M., Lawrence, K.T., Liu, Z., Dekens, P.S., Ravelo, A.C., 2013. Patterns and mechanisms of early Pliocene warmth. Nature 496, 43–49. http://dx.doi.org/10.1038/nature12003.
Flesche Kleiven, H., Jansen, E., Fronval, T., Smith, T., 2002. Intensification of Northern Hemisphere glaciations in the circum Atlantic region (3.5–2.4 Ma) – ice-rafted detritus evidence. Palaeogeogr. Palaeoclimatol. Palaeoecol. 184, 213–223. http://dx.doi.org/10.1016/S0031-0182(01)00407-2.
Frank, M., Reynolds, B.C., Keith O'Nions, R., Nions, R.K.O., 1999. Nd and Pb isotopes in Atlantic and Pacific water masses before and after closure of the Panama gateway. Geology 27, 1147. http://dx.doi.org/10.1130/0091-7613(1999)027<1147:NAPIIA>2.3.CO;2.
Ganopolski, A., Calov, R., 2011. The role of orbital forcing, carbon dioxide and regolith in 100 kyr glacial cycles. Clim. Past 7, 1415–1425. http://dx.doi.org/10.5194/cp-7-1415-2011.
Ganopolski, A., Rahmstorf, S., 2001. Rapid changes of glacial climate simulated in a coupled climate model. Nature 409, 153–158. http://dx.doi.org/10.1038/35051500.
Ganopolski, A., Rahmstorf, S., 2002. Abrupt glacial climate changes due to Stochastic resonance. Phys. Rev. Lett. 88, 038501. http://dx.doi.org/10.1103/PhysRevLett.88.038501.
Ganopolski, A., Roche, D.M., 2009. On the nature of lead–lag relationships during glacial–interglacial climate transitions. Quat. Sci. Rev. 28, 3361–3378. http://dx.doi.org/10.1016/j.quascirev.2009.09.019.
Ganopolski, A., Rahmstorf, S., Petoukhov, V., Claussen, M., 1998. Simulation of modern and glacial climates with a coupled global model of intermediate complexity. Nature 351–356.
Ganopolski, A., Petoukhov, V., Rahmstorf, S., Brovkin, V., Claussen, M., Eliseev, A., Kubatzki, C., 2001. CLIMBER-2: a climate system model of intermediate complexity. Part II: model sensitivity. Clim. Dyn. 17, 735–751. http://dx.doi.org/10.1007/s003820000144.
Ganopolski, A., Calov, R., Claussen, M., 2010. Simulation of the last glacial cycle with a coupled climate ice-sheet model of intermediate complexity. Clim. Past 6, 229–244. http://dx.doi.org/10.5194/cp-6-229-2010.
Greve, R., 1997. Application of a polythermal three-dimensional ice sheet model to the Greenland ice sheet: response to steady-state and transient climate scenarios. J. Clim. 901–918.
Harrison, T.M., Copeland, P., Kidd, W.S., Yin, A., 1992. Raising tibet. Science 255, 1663–1670. http://dx.doi.org/10.1126/science.255.5052.1663.
Haug, G.H., Tiedemann, R., 1998. Effect of the formation of the Isthmus of Panama on Atlantic Ocean thermohaline circulation. Nature 393, 673–676. http://dx.doi.org/10.1038/31447.
Haug, G.H., Sigman, D.M., Tiedemann, R., Pedersen, T.F., Sarnthein, M., 1999. Onset of permanent stratification in the subarctic. Pac. Ocean 401, 779–782. http://dx.doi.org/10.1038/44550.
Haug, G.H., Tiedemann, R., Zahn, R., Ravelo, A.C., 2001. Role of Panama uplift on oceanic freshwater balance. Geology 29, 207–210. http://dx.doi.org/10.1130/0091-7613(2001)029.
Haug, G.H., Ganopolski, A., Sigman, D.M., Rosell-Mele, A., Swann, G.E.A., Tiedemann, R., Jaccard, S.L., Bollmann, J., Maslin, M.A., Leng, M.J., Eglinton, G., 2005. North Pacific seasonality and the glaciation of North America 2.7 million years ago. Nature 433, 821–825. http://dx.doi.org/10.1038/nature03332.

Hay, W.W., 1992. The cause of the Late Cenozoic Northern Hemisphere glaciations: a climate change enigma. Terra Nov. 4, 305–311. http://dx.doi.org/10.1111/j.1365-3121.1992.tb00819.x.
Haywood, A.M., Valdes, P.J., 2004. Modelling Pliocene warmth: contribution of atmosphere, oceans and cryosphere. Earth Planet. Sci. Lett. 218, 363–377. http://dx.doi.org/10.1016/S0012-821X(03)00685-X.
Haywood, A.M., Hill, D.J., Dolan, A.M., Otto-Bliesner, B.L., Bragg, F., Chan, W.-L., Chandler, M.A., Contoux, C., Dowsett, H.J., Jost, A., Kamae, Y., Lohmann, G., Lunt, D.J., Abe-Ouchi, A., Pickering, S.J., Ramstein, G., Rosenbloom, N.A., Salzmann, U., Sohl, L., Stepanek, C., Ueda, H., Yan, Q., Zhang, Z., 2013. Large-scale features of Pliocene climate: results from the Pliocene Model Intercomparison Project. Clim. Past 8, 191–209. http://dx.doi.org/10.5194/cp-9-191-2013.
Herbert, T.D., Peterson, L.C., Lawrence, K.T., Liu, Z., 2010. Tropical ocean temperatures over the past 3.5 million years. Science 328, 1530–1534. http://dx.doi.org/10.1126/science.1185435.
Hönisch, B., Hemming, N.G., Archer, D., Siddall, M., McManus, J.F., 2009. Atmospheric carbon dioxide concentration across the mid-Pleistocene transition. Science 324, 1551–1554. http://dx.doi.org/10.1126/science.1171477.
Hutter, K., 1983. Theoretical Glaciology: Material Science of Ice and the Mechanics of Glaciers and Ice Sheets. Reidel.
James, N.P., Bone, Y., Carter, R.M., Murray-Wallace, C.V., 2006. Origin of the Late Neogene Roe Plains and their calcarenite veneer: implications for sedimentology and tectonics in the Great Australian Bight. Aust. J. Earth Sci. 53, 407–419. http://dx.doi.org/10.1080/08120090500499289.
Jansen, E., Sjøholm, J., 1991. Reconstruction of glaciation over the past 6 Myr from ice-borne deposits in the Norwegian Sea. Nature 349, 600–603. http://dx.doi.org/10.1038/349600a0.
Jansen, E., Fronval, T., Rack, F., Channell, J.E.T., 2000. Pliocene-Pleistocene ice rafting history and cyclicity in the Nordic Seas during the last 3.5 Myr. Paleoceanography 15, 709–721. http://dx.doi.org/10.1029/1999PA000435.
Kaufman, D., Brigham-Grette, J., 1993. Aminostratigraphic correlations and paleotemperature implications, Pliocene-Pleistocene high-sea-level deposits, northwestern Alaska. Quat. Sci. Rev. 12, 21–33.
Keigwin, L.D.J., 1978. Pliocene closing of the Isthmus of Panama, based on biostratigraphic evidence from nearby Pacific Ocean and Caribbean Sea cores. Geology 6, 630–634. http://dx.doi.org/10.1130/0091-7613(1978)6.
Keigwin, L., 1982. Isotopic paleoceanography of the Caribbean and East pacific: role of panama uplift in late neogene time. Science 217, 350–353. http://dx.doi.org/10.1126/science.217.4557.350.
Keller, G., Zenker, C.E., Stone, S.M., 1989. Late neogene history of the Pacific-Caribbean gateway. J. South Am. Earth Sci. 2, 73–108.
Krantz, D., 1991. A chronology of Pliocene sea-level fluctuations: the US Middle Atlantic Coastal Plain record. Quat. Sci. Rev. 10, 163–174.
Laskar, J., Robutel, P., Joutel, F., Gastineau, M., Correia, A.C.M., Levrard, B., 2004. A long-term numerical solution for the insolation quantities of the Earth. Astron. Astrophys. 428, 261–285. http://dx.doi.org/10.1051/0004-6361:20041335.
Lawrence, P.J., Chase, T.N., 2010. Investigating the climate impacts of global land cover change in the community climate system model. Int. J. Climatol. 30, 2066–2087. http://dx.doi.org/10.1002/joc.2061.
Lawrence, K.T., Liu, Z., Herbert, T.D., 2006. Evolution of the eastern tropical Pacific through Plio-Pleistocene glaciation. Science 312, 79–83. http://dx.doi.org/10.1126/science.1120395.
Lawrence, K.T., Herbert, T.D., Brown, C.M., Raymo, M.E., Haywood, A.M., 2009. High-amplitude variations in North Atlantic sea surface temperature during the early Pliocene warm period. Paleoceanography 24. http://dx.doi.org/10.1029/2008PA001669 n/a–n/a.
Lawrence, K.T., Sosdian, S., White, H.E., Rosenthal, Y., 2010. North Atlantic climate evolution through the Plio-Pleistocene climate transitions. Earth Planet. Sci. Lett. 300, 329–342. http://dx.doi.org/10.1016/j.epsl.2010.10.013.
Li, X.S., Berger, A., Loutre, M.F., Maslin, M.A., Haug, G.H., Tiedemann, R., 1998. Simulating Late Pliocene northern hemisphere climate with the LLN 2-D Model. Geophys. Res. Lett. 25, 915–918. http://dx.doi.org/10.1029/98GL00443.
Li, L., Li, Q., Tian, J., Wang, P., Wang, H., Liu, Z., 2011. A 4-Ma record of thermal evolution in the tropical western Pacific and its implications on climate change. Earth Planet. Sci. Lett. 309, 10–20. http://dx.doi.org/10.1016/j.epsl.2011.04.016.
Lisiecki, L.E., Raymo, M.E., 2005. A Pliocene-Pleistocene stack of 57 globally distributed benthic δ 18 O records. Paleoceanography 20. http://dx.doi.org/10.1029/2004PA001071.
Lisiecki, L.E., Raymo, M.E., 2007. Plio-Pleistocene climate evolution: trends and transitions in glacial cycle dynamics. Quat. Sci. Rev. 26, 56–69. http://dx.doi.org/10.1016/j.quascirev.2006.09.005.
Lourens, L.J., Hilgen, F.J., 1997. Long-periodic variations in the Earth's obliquity and their relation to third-order eustatic cycles and late Neogene glaciations. Quat. Int. 40, 43–52.
Lunt, D.J., de Noblet-Ducoudré, N., Charbit, S., Noblet-Ducoudre, N., 2004. Effects of a melted greenland ice sheet on climate, vegetation, and the cryosphere. Clim. Dyn. 23, 679–694. http://dx.doi.org/10.1007/s00382-004-0463-4.
Lunt, D.J., Foster, G.L., Haywood, A.M., Stone, E.J., 2008. Late Pliocene Greenland glaciation controlled by a decline in atmospheric CO_2 levels. Nature 454, 1102–1105. http://dx.doi.org/10.1038/nature07223.
Lunt, D.J., Haywood, A.M., Schmidt, G.A., Salzmann, U., Valdes, P.J., Dowsett, H.J., Loptson, C.A., 2012. On the causes of mid-Pliocene warmth and polar amplification. Earth Planet. Sci. Lett. 321–322, 128–138. http://dx.doi.org/10.1016/j.epsl.2011.12.042.
Mann, P., Corrigan, J., 1990. Model for late Neogene deformation in Panama. Geology 18, 558–562. http://dx.doi.org/10.1130/0091-7613(1990)018.
Marchitto, T.M., Curry, W.B., Lynch-Stieglitz, J., Bryan, S.P., Cobb, K.M., Lund, D.C., 2014. Improved oxygen isotope temperature calibrations for cosmopolitan benthic foraminifera. Geochim. Cosmochim. Acta 130, 1–11. http://dx.doi.org/10.1016/j.gca.2013.12.034.
Martínez-Botí, M. a., Foster, G.L., Chalk, T.B., Rohling, E.J., Sexton, P.F., Lunt, D.J., Pancost, R.D., Badger, M.P.S., Schmidt, D.N., 2015. Plio-Pleistocene climate sensitivity evaluated using high-resolution CO_2 records. Nature 518, 49–54. http://dx.doi.org/10.1038/nature14145.
Martínez-Garcia, A., Rosell-Melé, A., McClymont, E.L., Gersonde, R., Haug, G.H., 2010. Subpolar link to the emergence of the modern equatorial Pacific cold tongue. Science 328, 1550–1553. http://dx.doi.org/10.1126/science.1184480.
Maslin, M., Haug, G., Sarnthein, M., Tiedemann, R., Erlenkeuser, H., Stax, R., 1992. Northwest Pacific Site 882: the initiation of northern Hemisphere glaciation. Proc. Ocean. Drill. Program, Sci. Results 145, 315–329.
Maslin, M.A., Haug, G.H., Sarnthein, M., Tiedemann, R., 1996. The progressive intensification of northern hemisphere glaciation as seen from the. North Pac. Geol. Rundsch. 85, 452–465. http://dx.doi.org/10.1007/s005310050088.
Maslin, M.A., Li, X.S., Loutre, M.-F., Berger, A., 1998. The contribution of orbital forcing to the progressive intensification of Northern Hemisphere glaciation. Quat. Sci. Rev. 17, 411–426. http://dx.doi.org/10.1016/S0277-3791(97)00047-4.
Masson-Delmotte, V., Schulz, M., Abe-Ouchi, A., Beer, J., Ganopolski, A., Rouco, J.F.G., Jansen, E., Lambeck, K., Luterbacher, J., Naish, T., Osborn, T., Otto-Bliesner, B., Quinn, T., Ramesh, R., Rojas, M., Shao, X., Timmermann, A., Uk, D.F., Uk, G.F., Zealand, N., France, M.K., 2013. Information from Paleoclimate Archives. In: Stocker, T.F., Qin, D., Plattner, G.-K., Tignor, M., Allen, S.K., Boschung, J., Nauels, A., Xia, Y., Bex, V., Midgley, P.M. (Eds.), Climate Change 2013: the Physical Science Basis. Contribution of Working Group I to the Fifth Assessment Report of the Intergovernmental Panel on Climate Change. Cambridge University Press, Cambridge, United Kingdom and New York, NY, USA.
Medina-Elizalde, M., Lea, D.W., Fantle, M.S., 2008. Implications of seawater Mg/Ca variability for Plio-Pleistocene tropical climate reconstruction. Earth Planet. Sci. Lett. 269, 585–595. http://dx.doi.org/10.1016/j.epsl.2008.03.014.
Milankovitch, M., 1941. Kanon der Erdbestrahlung und seine Anwendung auf das Eiszeitenproblem. Mihaila Ćurcića, Belgrade.
Miller, K.G., Wright, J.D., Browning, J.V., Kulpecz, A., Kominz, M., Naish, T.R., Cramer, B.S., Rosenthal, Y., Peltier, W.R., Sosdian, S., 2012. High tide of the warm Pliocene: implications of global sea level for Antarctic deglaciation. Geology 40, 407–410. http://dx.doi.org/10.1130/G32869.1.
Molnar, P., England, P., 1990. Late Cenozoic uplift of mountain ranges and global climate change: chicken or egg? Nature 346, 29–34. http://dx.doi.org/10.1038/346029a0.
Montes, C., Cardona, A., Jaramillo, C., Pardo, A., Silva, J.C., Valencia, V., Ayala, C., Perez-Angel, L.C., Rodriguez-Parra, L.A., Ramirez, V., Nino, H., 2015. Middle Miocene closure of the Central American Seaway. Science 348, 226–229. http://dx.doi.org/10.1126/science.aaa2815.
Morland, L.W., 1984. Thermomechanical balances of ice sheet flows. Geophys. Astrophys. Fluid Dyn. 29, 237–266. http://dx.doi.org/10.1080/03091928408248191.
Mudelsee, M., Raymo, M.E., 2005. Slow dynamics of the Northern Hemisphere glaciation. Paleoceanography 20. http://dx.doi.org/10.1029/2005PA001153 n/a–n/a.
Naafs, B.D.A., Stein, R., Hefter, J., Khélifi, N., De Schepper, S., Haug, G.H., 2010. Late Pliocene changes in the North Atlantic Current. Earth Planet. Sci. Lett. 298, 434–442. http://dx.doi.org/10.1016/j.epsl.2010.08.023.
Naafs, B.D.A., Hefter, J., Acton, G., Haug, G.H., Martínez-Garcia, A., Pancost, R., Stein, R., 2012. Strengthening of North American dust sources during the late Pliocene (2.7 Ma). Earth Planet. Sci. Lett. 317–318, 8–19. http://dx.doi.org/10.1016/j.epsl.2011.11.026.
Naish, T.R., Wilson, G.S., 2009. Constraints on the amplitude of Mid-Pliocene (3.6–2.4 Ma) eustatic sea-level fluctuations from the New Zealand shallow-marine sediment record. Philos. Trans. A. Math. Phys. Eng. Sci. 367, 169–187. http://dx.doi.org/10.1098/rsta.2008.0223.
Naish, T., Powell, R., Levy, R., Wilson, G., Scherer, R., Talarico, F., Krissek, L., Niessen, F., Pompilio, M., Wilson, T., Carter, L., DeConto, R., Huybers, P., McKay, R., Pollard, D., Ross, J., Winter, D., Barrett, P., Browne, G., Cody, R., Cowan, E., Crampton, J., Dunbar, G., Dunbar, N., Florindo, F., Gebhardt, C., Graham, I., Hannah, M., Hansaraj, D., Harwood, D., Helling, D., Henrys, S., Hinnov, L., Kuhn, G., Kyle, P., Läufer, A., Maffioli, P., Magens, D., Mandernack, K., McIntosh, W., Millan, C., Morin, R., Ohneiser, C., Paulsen, T., Persico, D., Raine, I., Reed, J., Riesselman, C., Sagnotti, L., Schmitt, D., Sjunneskog, C., Strong, P., Taviani, M., Vogel, S., Wilch, T., Williams, T., 2009. Obliquity-paced Pliocene West Antarctic ice sheet oscillations. Nature 458, 322–328. http://dx.doi.org/10.1038/nature07867.
Pagani, M., Liu, Z., LaRiviere, J., Ravelo, A.C., 2010. High Earth-system climate sensitivity determined from Pliocene carbon dioxide concentrations. Nat. Geosci. 3, 27–30. http://dx.doi.org/10.1038/ngeo724.
Petoukhov, V., Ganopolski, A., Brovkin, V., Claussen, M., Eliseev, A., Kubatzki, C., Rahmstorf, S., 2000. CLIMBER-2: a climate system model of intermediate complexity. Part I: model description and performance for present climate. Clim. Dyn. 16, 1–17. http://dx.doi.org/10.1007/PL00007919.
Philander, S.G., Fedorov, A.V., 2003. Role of tropics in changing the response to Milankovich forcing some three million years ago. Paleoceanography 18. http://dx.doi.org/10.1029/2002PA000837 n/a–n/a.

Pollard, D., DeConto, R.M., 2009. Modelling West Antarctic ice sheet growth and collapse through the past five million years. Nature 458, 329–332. http://dx.doi.org/10.1038/nature07809.
Quade, J., Cerling, T.E., Bowman, J.R., 1989. Development of Asian monsoon revealed by marked ecological shift during the latest Miocene in northern Pakistan. Nature 342, 163–166. http://dx.doi.org/10.1038/342163a0.
Raymo, M.E., 1991. Geochemical evidence supporting T. C. Chamberlin's theory of glaciation. Geology 19, 344–347. http://dx.doi.org/10.1130/0091-7613(1991)019.
Raymo, M., 1994a. The Himalayas, organic carbon burial, and climate in the Miocene. Paleoceanography 9, 399–404.
Raymo, M.E., 1994b. The initiation of northern hemisphere glaciation. Annu. Rev. Earth Planet. Sci. 22, 353–383. http://dx.doi.org/10.1146/annurev.ea.22.050194.002033.
Raymo, M.E., Nisancioglu, K., 2003. The 41 kyr world: Milankovitch's other unsolved mystery. Paleoceanography 18. http://dx.doi.org/10.1029/2002PA000791 n/a–n/a.
Raymo, M.E., Ruddiman, W.F., 1992. Tectonic forcing of late Cenozoic climate. Nature 359, 117–122. http://dx.doi.org/10.1038/359117a0.
Raymo, M.E., Ruddiman, W.F., Froelich, P.N., 1988. Influence of late Cenozoic mountain building on ocean geochemical cycles. Geology 16, 649–653. http://dx.doi.org/10.1130/0091-7613(1988)016.
Raymo, M., Grant, B., Horowitz, M., Rau, G., 1996. Mid-Pliocene warmth: stronger greenhouse and stronger conveyor. Mar. Micropaleontol. 27.
Raymo, M., Lisiecki, L., Nisancioglu, K., 2006. Plio-Pleistocene Ice Volume, Antarctic climate, and the global $d^{18}O$ record. Science 313, 492–495.
Raymo, M.E., Mitrovica, J.X., O'Leary, M.J., DeConto, R.M., Hearty, P.J., 2011. Departures from eustasy in Pliocene sea-level records. Nat. Geosci. 4, 328–332. http://dx.doi.org/10.1038/ngeo1118.
Robinson, A., Calov, R., Ganopolski, A., 2010. An efficient regional energy-moisture balance model for simulation of the Greenland Ice Sheet response to climate change. Cryosph. 4, 129–144. http://dx.doi.org/10.5194/tc-4-129-2010.
Robinson, A., Calov, R., Ganopolski, A., 2011. Greenland ice sheet model parameters constrained using simulations of the Eemian Interglacial. Clim. Past 7, 381–396. http://dx.doi.org/10.5194/cp-7-381-2011.
Robinson, A., Calov, R., Ganopolski, A., 2012. Multistability and critical thresholds of the Greenland ice sheet. Nat. Clim. Chang. 2, 429–432. http://dx.doi.org/10.1038/nclimate1449.
Rohling, E.J., Foster, G.L., Grant, K.M., Marino, G., Roberts, A.P., Tamisiea, M.E., Williams, F., 2014. Sea-level and deep-sea-temperature variability over the past 5.3 million years. Nature 508, 477–482. http://dx.doi.org/10.1038/nature13230.
Rowley, D.B., Forte, A.M., Moucha, R., Mitrovica, J.X., Simmons, N.A., Grand, S.P., 2013. Dynamic topography change of the eastern United States since 3 million years ago. Science 340, 1560–1563. http://dx.doi.org/10.1126/science.1229180.
Ruddiman, W.F., 2003. Orbital insolation, ice volume, and greenhouse gases. Quat. Sci. Rev. 22, 1597–1629. http://dx.doi.org/10.1016/S0277-3791(03)00087-8.
Ruddiman, W.F., 2004. The role of greenhouse gases in orbital-scale climatic changes. Eos, Trans. Am. Geophys. Union 85, 1. http://dx.doi.org/10.1029/2004EO010002.
Ruddiman, W.F., Kutzbach, J.E., 1991. Plateau uplift and climatic change. Sci. Am. 264, 66–75. http://dx.doi.org/10.1038/scientificamerican0391-66.
Ruddiman, W.F., Raymo, M.E., Lamb, H.H., Andrews, J.T., 1988. Northern hemisphere climate regimes during the past 3 Ma: possible tectonic connections [and Discussion]. Philos. Trans. R. Soc. B Biol. Sci. 318, 411–430. http://dx.doi.org/10.1098/rstb.1988.0017.
Ruddiman, F., Kutzbach, J.E., America, N., Ruddiman, W.F., 1989. Forcing of late Cenozoic northern hemisphere climate by plateau uplift in southern Asia and the American west. J. Geophys. Res. 94, 18409. http://dx.doi.org/10.1029/JD094iD15p18409.
Seki, O., Foster, G.L., Schmidt, D.N., Mackensen, A., Kawamura, K., Pancost, R.D., 2010. Alkenone and boron-based Pliocene pCO_2 records. Earth Planet. Sci. Lett. 292, 201–211. http://dx.doi.org/10.1016/j.epsl.2010.01.037.
Shackleton, N., 1974. Attainment of Isotopic Equilibrium between Ocean Water and the Benthonic Foraminifera Genus Uvigerina: Isotopic Changes in the Ocean during the Last Glacial, Colloques Internationaux du C.N.R.S. N° 219.
Shackleton, N.J., Hall, M.A., Pate, D., 1995. Pliocene stable isotope stratigraphy of site 846 138, pp. 337–355.
Sigman, D., Jaccard, S., Haug, G., 2004. Polar ocean stratification in a cold climate. Nature 428, 59–63. http://dx.doi.org/10.1038/nature02378.1.
Sosdian, S., Rosenthal, Y., 2009. Deep-sea temperature and ice volume changes across the Pliocene-Pleistocene climate transitions. Science 325, 306–310. http://dx.doi.org/10.1126/science.1169938.
Studer, A.S., Martínez-Garcia, A., Jaccard, S.L., Girault, F.E., Sigman, D.M., Haug, G.H., 2012. Enhanced stratification and seasonality in the Subarctic Pacific upon Northern Hemisphere Glaciation – new evidence from diatom-bound nitrogen isotopes, alkenones and archaeal tetraethers. Earth Planet. Sci. Lett. 351–352, 84–94. http://dx.doi.org/10.1016/j.epsl.2012.07.029.
Taylor, K.E., 2001. Summarizing multiple aspects of model performance in a single diagram. J. Geophys. Res. 106, 7183. http://dx.doi.org/10.1029/2000JD900719.
Toniazzo, T., Gregory, J.M., Huybrechts, P., 2004. Climatic impact of a Greenland Deglaciation and its possible irreversibility. J. Clim. 17, 21–33. http://dx.doi.org/10.1175/1520-0442(2004)017<0021:CIOAGD>2.0.CO;2.
Uppala, S.M., Kållberg, P.W., Simmons, A.J., Andrae, U., Bechtold, V.D.C., Fiorino, M., Gibson, J.K., Haseler, J., Hernandez, A., Kelly, G.A., Li, X., Onogi, K., Saarinen, S., Sokka, N., Allan, R.P., Andersson, E., Arpe, K., Balmaseda, M.A., Beljaars, A.C.M., Van De, Berg, L., Bidlot, J., Bormann, N., Caires, S., Chevallier, F., Dethof, A., Dragosavac, M., Fisher, M., Fuentes, M., Hagemann, S., Hólm, E., Hoskins, B.J., Isaksen, L., Janssen, P.A.E.M., Jenne, R., Mcnally, A.P., Mahfouf, J.-F., Morcrette, J.-J., Rayner, N.A., Saunders, R.W., Simon, P., Sterl, A., Trenberth, K.E., Untch, A., Vasiljevic, D., Viterbo, P., Woollen, J., 2005. The ERA-40 re-analysis. Q. J. R. Meteorol. Soc. 131, 2961–3012. http://dx.doi.org/10.1256/qj.04.176.
Van de Wal, R.S.W., de Boer, B., Lourens, L.J., Köhler, P., Bintanja, R., 2011. Reconstruction of a continuous high-resolution CO_2 record over the past 20 million years. Clim. Past 7, 1459–1469. http://dx.doi.org/10.5194/cp-7-1459-2011.
Venti, N.L., Billups, K., Herbert, T.D., 2013. Increased sensitivity of the Plio-Pleistocene northwest Pacific to obliquity forcing. Earth Planet. Sci. Lett. 384, 121–131. http://dx.doi.org/10.1016/j.epsl.2013.10.007.
Wara, M.W., Ravelo, A.C., Delaney, M.L., 2005. Permanent El Niño-like conditions during the Pliocene warm period. Science 309, 758–761. http://dx.doi.org/10.1126/science.1112596.
Wardlaw, B., Quinn, T., 1991. The record of Pliocene sea-level change at Enewetak Atoll. Quat. Sci. Rev. 10, 247–258.
Willeit, M., Ganopolski, A., Feulner, G., 2013. On the effect of orbital forcing on mid-Pliocene climate, vegetation and ice sheets. Clim. Past 9, 1749–1759. http://dx.doi.org/10.5194/cp-9-1749-2013.
Willenbring, J.K., von Blanckenburg, F., 2010. Long-term stability of global erosion rates and weathering during late-Cenozoic cooling. Nature 465, 211–214. http://dx.doi.org/10.1038/nature09044.
Williams, T., van de Flierdt, T., Hemming, S.R., Chung, E., Roy, M., Goldstein, S.L., 2010. Evidence for iceberg armadas from East Antarctica in the Southern Ocean during the late Miocene and early Pliocene. Earth Planet. Sci. Lett. 290, 351–361. http://dx.doi.org/10.1016/j.epsl.2009.12.031.
Woodard, S.C., Rosenthal, Y., Miller, K.G., Wright, J.D., Chiu, B.K., Lawrence, K.T., 2014. Antarctic role in Northern Hemisphere glaciation. Science 847. http://dx.doi.org/10.1126/science.1255586.
Wright, J.D., Miller, K.G., 1996. Control of North Atlantic deep water circulation by the Greenland-Scotland Ridge. Paleoceanography 11, 157–170. http://dx.doi.org/10.1029/95PA03696.